Inorganic Chemistry

pubs.acs.org/IC

Article

# Charge-Transfer Spectroscopy of Bisaxially Coordinated Iron(II) Phthalocyanines through the Prism of the Lever's $E_L$ Parameters Scale, MCD Spectroscopy, and TDDFT Calculations

Dustin E. Nevonen, Laura S. Ferch, Briana R. Schrage, and Victor N. Nemykin*

Cite This: *Inorg. Chem.* 2022, 61, 8250−8266

Read Online

ACCESS | Metrics & More | Article Recommendations | Supporting Information

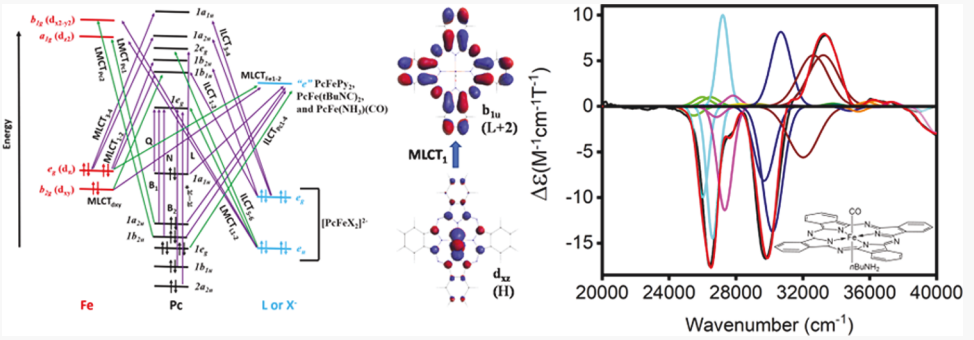


**ABSTRACT:** The position of the experimentally observed (in the UV−vis and magnetic circular dichroism (MCD) spectra) low-energy metal-to-ligand charge-transfer (MLCT) band in low-spin iron(II) phthalocyanine complexes of general formula $PcFeL_2$, PcFeL′L″, and $[PcFeX_2]^{2-}$ (L, L′, or L″ are neutral and $X^-$ is an anionic axial ligand) was correlated with the Lever's electrochemical $E_L$ scale values for the axial ligands. The time-dependent density functional theory (TDDFT)-predicted UV−vis spectra are in very good agreement with the experimental data for all complexes. In the majority of compounds, TDDFT predicts that the first degenerate MLCT band that correlates with the MCD *A*-term observed between 360 and 480 nm is dominated by an $e_g$ (Fe, $d_\pi$) → $b_{1u}$ (Pc, $\pi^*$) single-electron excitation (in traditional $D_{4h}$ point group notation) and agrees well with the previous assignment discussed by Stillman and co-workers[*Inorg. Chem.* **1994**, *33*, 573−583]. The TDDFT calculations also suggest a small energy gap for $b_{1u}/b_{2u}$ (Pc, $\pi^*$) orbital splitting and closeness of the $MLCT_1$ $e_g$ (Fe, $d_\pi$) → $b_{1u}$ (Pc, $\pi^*$) and $MLCT_2$ $e_g$ (Fe, $d_\pi$) → $b_{2u}$ (Pc, $\pi^*$) transitions. In the case of the $PcFeL_2$ complexes with phosphines as the axial ligands, additional degenerate charge-transfer transitions were observed between 450 and 500 nm. These transitions are dominated by $a_{2u}$ (Pc + L, $\pi$) → $e_g$ (Pc, $\pi^*$) single-electron excitations and are unique for the $PcFe(PR_3)_2$ complexes. The energy of the phthalocyanine-based $a_{2u}$ orbital has large axial ligand dependency and is the reason for a large energy deviation for B1 $a_{2u}$ (Pc + L, $\pi$) → $e_g$ (Pc, $\pi^*$) transition. The energies of the axial ligand-to-iron, axial ligand-to-phthalocyanine, iron-to-axial ligand, and phthalocyanine-to-axial ligand charge-transfer transitions were discussed on the basis of TDDFT calculations.



## INTRODUCTION

Iron phthalocyanine derivatives and their analogues are known for their diversity in oxidation and spin states that range between +1 and +4, and 0 and 5/2, respectively.[1−6] Not surprisingly, such rich electronic structure properties, along with the complex coordination chemistry of iron phthalocyanine, resulted in the usage of these platforms as naked eye detectors of carbon monoxide and $NO_x$ species,[7−11] oxidative catalysts in transformations of organic molecules,[12−22] electrocatalysts,[23−25] reactive oxygen species activators in catalytic cancer therapy,[26,27] and smart electrode materials for the detection of biologically important molecules using electrochemical techniques.[28−31] The ability of the iron(II) phthalocyanine to coordinate two axial ligands such as the isonitriles,[32−38] nitroso compounds,[39] carbon monoxide,[40−42] phosphines and phosphites,[39,43−47] sulfides and sulfoxides,[48−50] and nitrogen bases[51−72] was studied by Mössbauer, NMR, UV−vis, and magnetic circular dichroism (MCD) spectroscopies as well as X-ray crystallography. In 1968, Dale reported the first paper on the UV−vis spectra of the $PcFeL_2$ and $[PcFeX_2]^{2-}$ complexes in which he suggested that the characteristic absorption band observed between 420 and 455 nm has a strong axial ligand dependency and thus can be

**Received:** March 3, 2022
**Published:** May 13, 2022

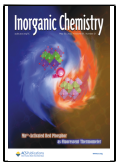




https://doi.org/10.1021/acs.inorgchem.2c00721
*Inorg. Chem.* 2022, 61, 8250−8266

attributed to the metal-to-ligand charge-transfer (MLCT) transition.[53] The first MCD work on these compounds was reported by Thomson and Stillman in 1974.[62] In their classic 1994 work,[61] Stillman and co-workers studied several $PcFeL_2$, $PcFeL'L''$, and $[PcFeX_2]^{2-}$ complexes (L, = $NH_3$, piperidine, *N*-methylimidazole, imidazole, pyridine, 4-methylpyridine; L′ = $NH_3$ and L″ = CO; and X = $CN^-$) using simultaneous band deconvolution analysis of the UV−vis and MCD spectra. Stillman proposed that the first (lowest-energy), axial ligand-dependent, MCD Faraday *A*-term observed in the 455−360 nm region is dominated by the $e_g$ ($d_{xz}/d_{yz}$) → $1b_{1u}$ (Pc, $\pi^*$) single-electron transition and mostly reflects the relative energy of the iron-centered $d_\pi$ orbitals (Figure 1).

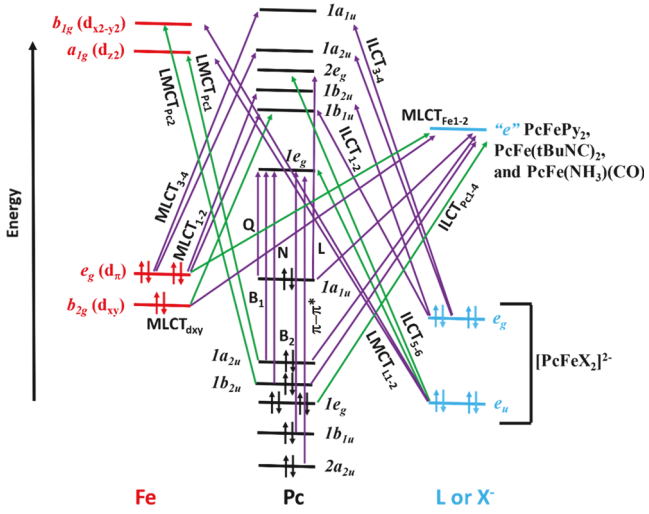


**Figure 1.** Selected arbitrary energy molecular diagram for the $^1A_{1g}$ ground state of $PcFeL_2$, $PcFeL'L''$, or $[PcFeX_2]^{2-}$ complex showing symmetry allowed metal-to-ligand charge-transfer (MLCT), ligand-to-metal charge-transfer (LMCT), phthalocyanine-centered, and inter-ligand charge-transfer (ILCT) transitions. (Right) Iron-centered molecular orbitals (MOs), (middle) phthalocyanine-centered MOs, and (left) axial ligand MOs. All labels except the "*e*" symmetry label for the unoccupied MO in the axial ligands are given for the idealized $D_{4h}$ point group. The *e* label reflects the lower DFT symmetry of the $PcFePy_2$, $PcFe(t\text{BuNC})_2$, and $PcFe(NH_3)(CO)$ complexes. Violet arrows represent *XY*-polarized transitions that give rise to MCD *A*-terms, and green arrows represent *Z*-polarized transitions that give rise to MCD *B*-terms.

Based on electrochemical, spectroelectrochemical, and chemical oxidation data, we have demonstrated recently that the energies of the iron(II) $d_\pi$ and $d_{xy}$ orbitals in $PcFeL_2$, $PcFeL'L''$, and $[PcFeX_2]^{2-}$ complexes have clear correlations with Lever's electrochemical $E_L$ parameter.[45] We also have shown that in the case of the axial ligands with moderate-to-strong $\pi$-acceptor character, iron-centered occupied MOs can intercross with the phthalocyanine-centered $a_{1u}$ (in the common Gouterman's notation for the $D_{4h}$ point group) orbital, which leads to the situation when the first oxidation process becomes phthalocyanine-centered.[45] We also observed rather unusual and rich UV−vis spectra for the $PcFeL_2$ complexes coordinated with the phosphine axial ligands. Our previous results pose several interesting questions. If the energy levels of the phthalocyanine ligand are nearly constant, as suggested by Lever's $E_L$ theory,[73−76] will the $[PcFeX_2]^{2-}$ complexes with the axial ligands having large negative $E_L$ values have the most red-shifted MLCT transitions? As of now, there are no reports available on the MCD spectroscopy of the bisaxially coordinated iron(II) phthalocyanines with negative values of the $\Sigma E_L$ L(ax) which are reflective of the high $\sigma$-donor strength of the axial ligands. Next, is the first (lowest-energy) MCD Faraday *A*-term in the 500−350 nm spectral envelope always associated with the $e_g$ (Fe, $d_\pi$) → $1b_{1u}$ (Pc, $\pi^*$) MLCT transition that correlates with the Lever's $E_L$ parameters? Finally, although numerical values for the UV−vis spectra of the $PcFeL_2$ complexes with several phosphines and phosphites as the axial ligands were reported in the literature,[43−47] no rational explanation of the nature of the observed transitions between 500 and 450 nm were ever provided and no MCD spectra for these $PcFeL_2$ compounds were ever reported. To answer the above-mentioned questions, we have conducted a systematic analysis of the UV−vis, MCD, DFT, and time-dependent density functional theory (TDDFT) data on a large range of $PcFeL_2$, $PcFeL'L''$, and $[PcFeX_2]^{2-}$ complexes (Figure 2), which, along with the earlier data from Stillman's and our group, allowed us to rationalize the spectroscopic behavior of these systems with respect to the Lever's $E_L$ ligand's parameter scale.[73−76]

Additive models for the correlation between the charge-transfer transition energies and coordination compounds' redox potentials are known for more than a half of century. Early analysis of the relationship between the oxidation potential or the difference of the first oxidation and the first reduction potentials and the energy of the charge-transfer transition was provided by Vlcek, Rabinowitch, Roothaan, Lever, and other authors.[77−103] In general, such plots are linear and can be described by the following equation for the series of homogeneous complexes[75]

$$E_{CT} = F(E_{Ox1} - E_{Red1}) + \sum a_i = F\Delta E + \text{const} \quad (1)$$

In the case of the lowest-energy metal-to-ligand charge-transfer (MLCT) transition that is dominated by the highest occupied molecular orbital (HOMO) → lowest unoccupied molecular orbital (LUMO) single-electron excitation (i.e., complete absence or small configuration interaction (CI) between MLCT and the other states of the same symmetry) without change in the overall spin of the system, $\Delta E$ in eq 1 represents the difference between the first metal-centered oxidation potential ($E_{Ox1}$) and the first ligand-centered reduction potential ($E_{Red1}$) scaled by the factor *F*, which may be at unity, but usually deviates from unity because of the functional dependence upon the electrochemical potentials. The term $\Sigma a_i$ usually includes molecular and solvent reorganization energies, electrostatic and entropic contributions, as well as other effects. In the case of the $PcFeL_2$, $PcFeL'L''$, and $[PcFeX_2]^{2-}$ complexes, eq 1 cannot be used as the lowest-energy MLCT band (i.e., $e_g$ (Fe, $d_\pi$) → $1e_g$ (Pc, $\pi^*$) in the standard notation for $D_{4h}$ point group, Figure 1) is symmetry forbidden and was not observed experimentally in the bisaxially coordinated unsubstituted iron(II) phthalocyanines. Thus, this transition will not be considered here.

Lever also has shown that when the first reduction potential of the ligand is unavailable, eq 2 still provides a good linear correlation between the MLCT energies of the ruthenium or iron complexes and the Ru(II)/Ru(III) or Fe(II)/Fe(III) oxidation potential[75,104]

$$E_{MLCT} = FE_{Ox1} + \text{const} \quad (2)$$


https://doi.org/10.1021/acs.inorgchem.2c00721
Inorg. Chem. 2022, 61, 8250−8266

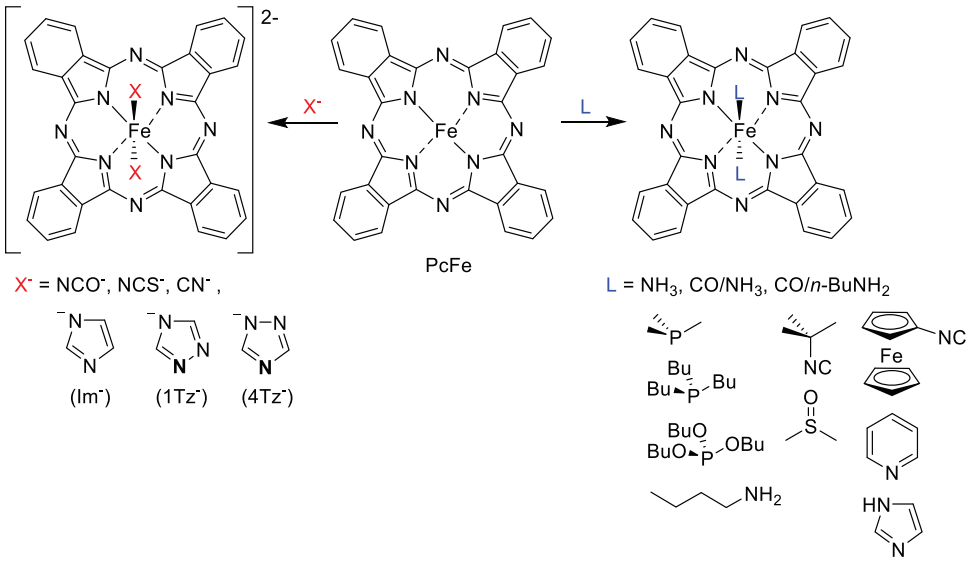


**Figure 2.** Structures of the axially ligated phthalocyanines featured in this work.

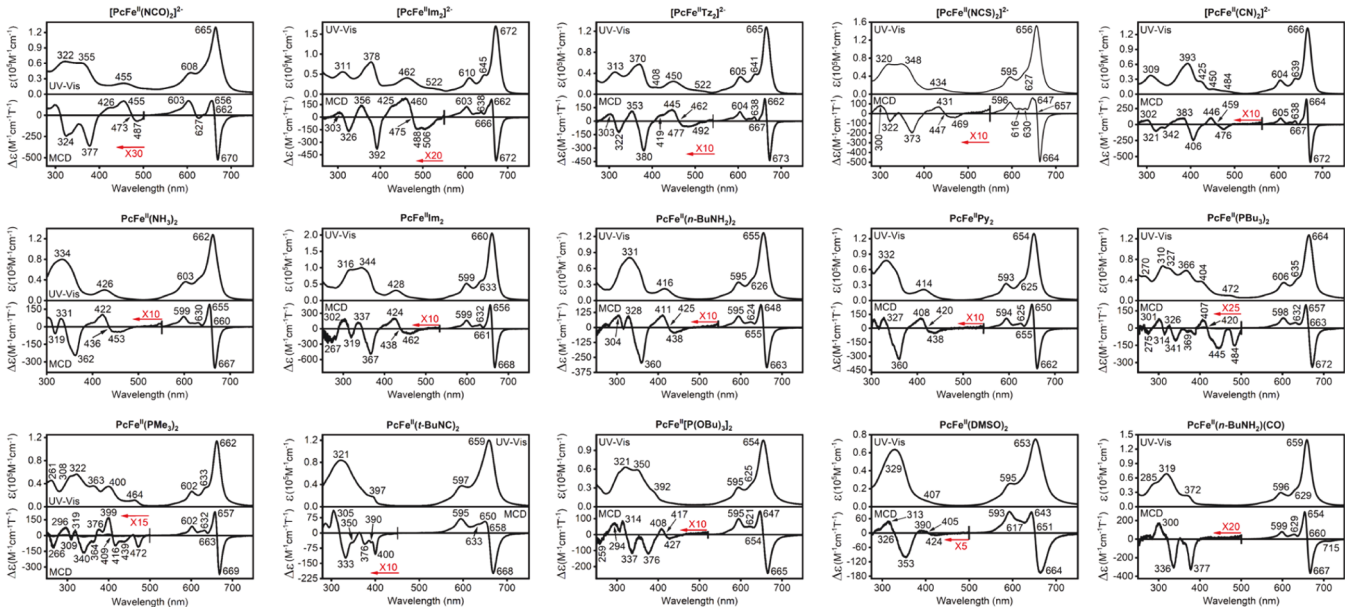


**Figure 3.** Experimental UV−vis and MCD spectra of all compounds evaluated in this work. Solvents: $[PcFeX_2]^{2-}$ (DMF for X = $NCO^-$, $Im^-$, $Tz^-$, $NCS^-$, and $CN^-$); DMSO for $PcFe(DMSO)_2$; dichloromethane (DCM) for all other compounds.

where all variables are the same as for eq 1 with constant $F$ being of nonunity value.

Since the Lever's $E_L$ parameters also should directly correlate with the values of $E_{Ox1}$ (i.e., energy of the HOMO in the homogeneous series of the complexes), one would expect that the MLCT energy should also correlate with the $E_L$ values in a linear way

$$E_{MLCT} = F \sum E_L + \text{const} \quad (3)$$

Finally, when applied to the homogeneous series of $PcFeL_2$, PcFeL′L″, and $[PcFeX_2]^{2-}$ complexes, following Lever's idea outlined earlier,[76] eq 3 can be rewritten as

$$E_{MLCT} = F \sum E_L L(ax) + \text{const} \quad (4)$$

where $\Sigma E_L$ L(ax) represents the sum of the $E_L$ values of two axial ligands. Equations 2 and 4 allow for tests of several hypotheses. First, eq 2 allows the linear correlation between $E_{MLCT}$ and $E_{Ox1}$ as long as the first oxidation process is metal-centered. As we have shown recently, the first oxidation process in the $PcFeL_2$ and PcFeL′L″ complexes with moderate-to-strong $\pi$-acceptors as the axial ligands, is phthalocyanine-centered. Thus, a significant deviation is expected for these compounds in their $E_{MLCT}/E_{Ox1}$ plot. On the other hand, eq 4 can predict the energies of the MLCT transitions in $PcFeL_2$, PcFeL′L″, and $[PcFeX_2]^{2-}$ complexes for which the Fe(II)/Fe(III) oxidation potentials are unavailable or hindered by the Pc(2−)/Pc(1−) process. In addition, eq 4 can be used in the analysis of the rather complex UV−vis and MCD spectra for $PcFeL_2$ complexes that are axially coordinated with phosphine ligands as well as the spectra of $[PcFe(CN)_2]^{2-}$ as it allows for the estimation of the energy of the $e_g$ (Fe, $d_\pi$) → $1b_{1u}$ (Pc, $\pi^*$) MLCT band.



https://doi.org/10.1021/acs.inorgchem.2c00721
Inorg. Chem. 2022, 61, 8250−8266

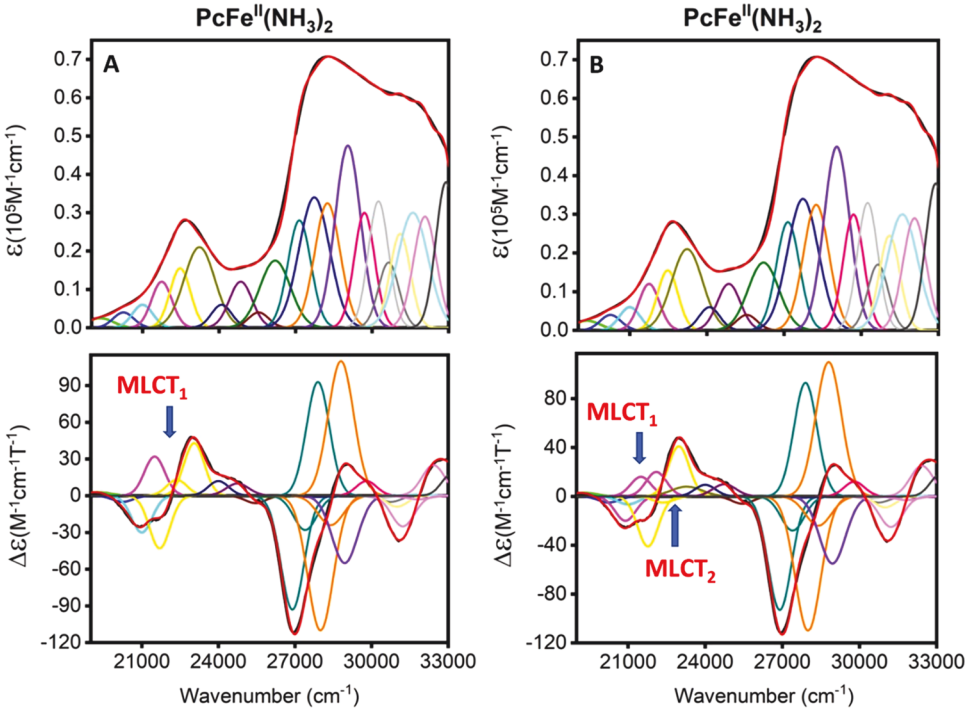


**Figure 4.** Deconvoluted UV−vis (top) and MCD (bottom) spectra for PcFe$(NH_3)_2$ using either (A) one *A*-term or (B) two *A*-terms in the MLCT region.

## RESULTS

**UV−Vis and MCD Spectra.** The UV−vis and MCD spectra of the 15 compounds discussed in this report are shown in Figure 3. When a comparison is possible with the MCD spectra of $PcFeL_2$, PcFeL′L″, and $[PcFeX_2]^{2-}$ complexes reported earlier by Stillman and co-workers,[61,62] our data are in excellent agreement for the $PcFePy_2$, $PcFe(Im)_2$, $PcFe(DMSO)_2$ and $[PcFe(CN)_2]^{2-}$ compounds. In general, all spectra can be roughly partitioned into three spectral envelopes. The first of which is the Q-band region (spectral envelope I; 500−750 nm), which for all compounds is dominated by a very intense Q-band observed between 653 and 672 nm. The energy of this transition is almost independent of the nature of the axial ligands or solvent ($\Delta E_Q \sim 400$ cm$^{-1}$), which is typical for phthalocyanine-centered $\pi-\pi^*$ transitions with negligible configurational interaction.[105] The energy of the Q-band observed in $PcFeL_2$, PcFeL′L″, and $[PcFeX_2]^{2-}$ complexes correlates well with the center of the only Faraday MCD *A*-term observed in the Q-band region, which confirms the effective fourfold symmetry of the phthalocyanine macrocycle. In addition, two vibronic satellites ($Q_{0-1}$ and $Q_{0-2}$) in spectral envelope I were also identified by UV−vis spectroscopy. These are associated with two MCD *B*-terms of positive amplitude and were observed earlier by Stillman and co-workers.[61,62] We assigned spectral envelope II to the 400−500 nm region. This region was traditionally associated with the MLCT ($e_g$ (Fe, $d_\pi$) → $1b_{1u}$ (Pc, $\pi^*$)) transitions.[53,61,62] With respect to spectral envelope II, the $PcFeL_2$, PcFeL′L″, and $[PcFeX_2]^{2-}$ complexes reported here can be consolidated into several groups. Group 1 ($PcFeL_2$, L = $NH_3$, Im, *n*$BuNH_2$, Py, $P(OBu)_3$, and dimethyl sulfoxide (DMSO); $[PcFeX_2]^{2-}$, X = $NCO^-$, $Im^-$, $Tz^-$, $NCS^-$) complexes have one band in their UV−vis spectrum (often with a shoulder) in this region, which correlates to some extent with a single visible MCD *A*-term. Group 2 ($PcFeL_2$, L = $PMe_3$, $PBu_3$, and $[PcFe(CN)_2]^{2-}$) has several observable bands in spectral envelope II in their UV−vis spectra. In the case of the phosphine-coordinated compounds, two MCD *A*-terms can be seen in the experimental MCD spectra, while only one MCD *A*-term can be seen in the experimental MCD spectrum of $[PcFe(CN)_2]^{2-}$ (Figure 3). Finally, group 3 ($PcFe(t$BuNC$)_2$ and $PcFe(n$BuNH$_2)$(CO) complexes) has no transitions in spectral envelope II. The third spectral envelope in the UV−vis and MCD spectra of the $PcFeL_2$, PcFeL′L″, and $[PcFeX_2]^{2-}$ complexes is located in the B-band region (250−400 nm). In the majority of cases, two main bands were observed in the UV−vis spectra within the B-band region (Figure 3). These bands are closely aligned with the two MCD *A*-terms. Again, more rich spectra were observed in the case of $PcFe(PR_3)_2$ and $[PcFe(CN)_2]^{2-}$ complexes.

**Band Deconvolution Analysis.** To interpret the several overlapping transitions present in their UV−vis and MCD spectra within the higher-energy charge-transfer region, band deconvolution analysis was performed for all compounds. In general, we used an approach very similar to that proposed by Stillman and co-workers.[61] Each of the signals in the deconvoluted UV−vis spectrum are energetically aligned with either a corresponding *A*- or *B*-term in the associated MCD spectrum. Sample deconvoluted spectra for the $PcFe(NH_3)_2$ complex in spectral envelopes II and III are shown in Figure 4.

When a comparison is possible (with the $PcFe(Im)_2$ and $PcFePy_2$ complexes), our data are in close agreement with those published by Stillman and co-workers.[61] In the case of the $[PcFe(CN)_2]^{2-}$ complex, we used an additional MCD *A*-term at around 425 nm to get a better agreement between theory and experiment. This observation is in agreement with the 1994 paper by Stillman and Ough.[61]

**DFT and TDDFT Calculations.** For electronic structure elucidation and to substantiate the experimental and deconvoluted UV−vis and MCD spectroscopy data, DFT


https://doi.org/10.1021/acs.inorgchem.2c00721
Inorg. Chem. 2022, 61, 8250−8266

and TDDFT calculations were performed on ten compounds that have $\Sigma E_L$ L(ax) values which span between −0.5 and +1.09 V. The relative energies of the phthalocyanine and iron-centered orbitals are expected to be dependent on the exchange−correlation functional used, with particular sensitivity to the magnitude of Hartree−Fock (HF) exchange involved in a given functional.[106−109] Therefore, the calculations were performed using the MPWLYP (5% Hartree−Fock exchange), TPSSh (10% Hartree−Fock exchange), and O3LYP (11.6% Hartree−Fock exchange) functionals. Although we focused on the three best-performing (for our purpose) exchange-correlation functionals, approximately 25 functionals were initially tested on a limited number of iron(II) phthalocyanine complexes. These functionals were selected for testing based on our experience with phthalocyanines[108] and success with using DFT calculations for the prediction of the redox events in iron(II) phthalocyanines.[45] As expected, the pure DFT functionals have historically underestimated the metal orbital energies in phthalocyanine systems, and hybrid functionals which have 20−42% HF exchange have been found to unreliably stabilize the d-orbitals of iron relative to the phthalocyanine core orbitals.

The associated DFT-predicted frontier molecular orbital images for selected examples $[PcFe(NCO)_2]^{2-}$ can be found in Figure 5, and the complete sets are located in Supporting

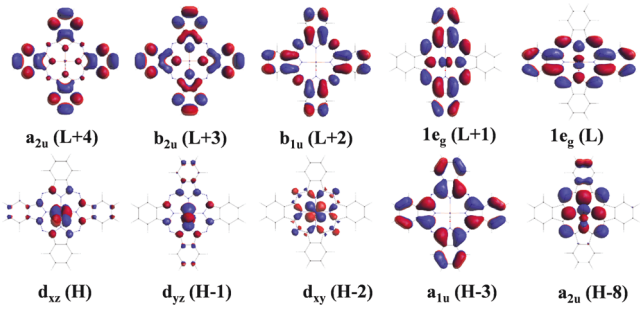


**Figure 5.** Select DFT-predicted frontier molecular orbitals for $[PcFe(NCO)_2]^{2-}$ complex calculated using the MPWLYP exchange-correlation functional.

Information Figure S1. The DFT-predicted energy-level diagram for all compounds using the MPWLYP exchange-correlation functional is presented in Figure 6, and those for the TPSSh and O3LYP functionals can be found in Supporting Information Figure S2. Within the energy-level diagram above, the compounds are ordered from low (negative) to high (positive) values of $\sum E_L$ L(ax) going from left to right on the *x*-axis. In all cases, the phthalocyanine-centered $e_g$ (in the traditional $D_{4h}$ point group notation) orbitals were identified as the LUMO and LUMO + 1, in agreement with the electrochemical data described earlier.[45] Again, in agreement with the previous electrochemical and spectroelectrochemical data,[45] iron-centered orbitals were identified as the HOMO in all complexes except for the cases of $PcFePy_2$, $PcFe[P(OMe)_3]_2$, $PcFe(DMSO)_2$, and $PcFe(NH_3)(CO)$ in which DFT predicts a phthalocyanine-centered $a_{1u}$ orbital to be the HOMO (Table 1). It is important to note (as it will be used in the TDDFT section discussion) that the classic Gouterman's[110−112] phthalocyanine-centered $a_{2u}$ orbital can be mixed with the $\sigma$-donor SALC orbital of the axial ligand. As a result, the axial ligands' contribution into this orbital was predicted between 11 and 64% (Supporting Information Table S1). For

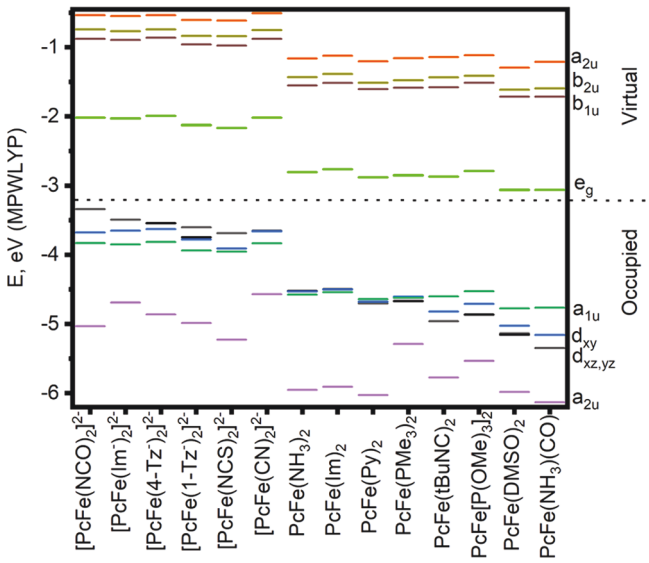


**Figure 6.** DFT-predicted (MPWLYP) energies of the selected orbitals for $PcFeL_2$, PcFeL′L″, and $[PcFeX_2]^{2-}$ complexes.

instance, in $[PcFe(Im^-)_2]^{2-}$, $PcFe(PMe_3)_2$, and $PcFe(DMSO)_2$ complexes, the axial ligand contribution to Gouterman's $a_{2u}$ orbital exceeds 50%. Such a large deviation in the axial ligand contribution to $a_{2u}$ orbital leads to a significant variation of the Gouterman's $a_{2u}$ orbital energy (Figure 6).

The TDDFT-predicted UV−vis spectra for all compounds using the MPWLYP exchange-correlation functional and DCM solvent are shown in Figure 7, and those for the TPSSh and O3LYP functionals can be located in Supporting Information Figure S3. In addition, the TDDFT-predicted spectra in DMF versus experimental spectra are also shown in Supporting Information Figure S3. The $PcFe(nBuNH_2)_2$, $PcFe(PBu_3)_2$, and $PcFe(nBuNH_2)(CO)$ complexes were not considered as their TDDFT-predicted spectra should be very close to those modeled for the $PcFe(NH_3)_2$, $PcFe(PMe_3)_2$, and $PcFe(NH_3)(CO)$ compounds, respectively. In each case, when compared to the O3LYP and TPSSh data, the MPWLYP calculations provided a slightly better general agreement with experiment in terms of predicted transition energies, intensities, and overall profile. The TDDFT-predicted properties of the selected excited states for all complexes are listed in Table 2, while complete data are present in Supporting Information Table S2.

In agreement with the experimental data, the energy deviation of the TDDFT-predicted Q-band in the $PcFeL_2$, PcFeL′L″, and $[PcFeX_2]^{2-}$ complexes is small (~500 $cm^{-1}$). Again, TDDFT calculations confirmed that the Q-band originates almost entirely from a $1a_{1u}$ (Pc, $\pi$) → $1e_g$ (Pc, $\pi^*$) single-electron transition.[110−112] In agreement with the earlier predictions by Stillman and co-workers,[61] TDDFT calculations identified the $MLCT_1$ and $MLCT_2$ bands as predominantly $e_g$ (Fe, $d_\pi$) → $1b_{1u}$ (Pc, $\pi^*$), and $e_g$ (Fe, $d_\pi$) → $1b_{2u}$ (Pc, $\pi^*$) single-electron excitations in character. The TDDFT-predicted energies of $MLCT_1$ and $MLCT_2$ have clear axial ligand dependency across the series ($\Delta E$ = ~9500 and ~9300 $cm^{-1}$, respectively). More interestingly, TDDFT calculations predicted that the $MLCT_1$ band in the $[PcFe(CN)_2]^{2-}$, $PcFeL_2$ (L = $PMe_3$, tBuNC, $P(OMe)_3$, and DMSO), and $PcFe(NH_3)(CO)$ complexes has a higher energy than the $B_1$ band (predominantly $1a_{2u}$ (Pc, $\pi$) → $1e_g$ (Pc, $\pi^*$) in character, Figure 1), which was not considered in the previous spectral


https://doi.org/10.1021/acs.inorgchem.2c00721
Inorg. Chem. 2022, 61, 8250−8266

**Table 1. Energies (in eV) of the Selected Frontier MOs in $PcFeL_2$, PcFeL′L″, and $[PcFeX_2]^{2-}$ Complexes (MPWLYP Functional)[a]**

| MO/L | $NCO^-$ | $Im^-$ | 1-$Tz^-$ | 4-$Tz^-$ | $NCS^-$ | $CN^-$ | $NH_3$ | Im | Py | $PMe_3$ | tBuNC | $P(OBu)_3$ | DMSO | $NH_3$/CO |
|---|---|---|---|---|---|---|---|---|---|---|---|---|---|---|
| $a_{1g}$ $d_{z^2}$ | −0.30 | −0.14 | −0.09 | −0.29 | −0.49 | −0.12 | −1.43 | −1.19 | −1.45 | −1.38 | −1.04 | −1.57 | −2.33 | −1.59 |
| $2e_g$ | −0.50 | −0.51 | −0.48 | −0.57 | −0.58 | −0.49 | −1.12 | −1.08 | −1.15 | −1.15 | −1.15 | −1.11 | −1.27 | −1.26 |
| $1a_{2u}$ | −0.53 | −0.55 | −0.53 | −0.60 | −0.62 | −0.51 | −1.16 | −1.12 | −1.21 | −1.16 | −1.14 | −1.12 | −1.30 | −1.21 |
| $1b_{2u}$ | −0.74 | −0.77 | −0.74 | −0.84 | −0.84 | −0.75 | −1.43 | −1.39 | −1.52 | −1.48 | −1.44 | −1.41 | −1.62 | −1.59 |
| $1b_{1u}$ | −0.88 | −0.89 | −0.86 | −0.96 | −0.98 | −0.88 | −1.55 | −1.52 | −1.60 | −1.59 | −1.58 | −1.52 | −1.72 | −1.71 |
| $1e_g$ | **−2.02** | **−2.03** | **−1.99** | **−2.12** | **−2.17** | **−2.02** | **−2.81** | **−2.76** | **−2.88** | **−2.85** | **−2.87** | **−2.79** | **−3.06** | **−3.06** |
| $e_g$ $d_\pi$ | **−3.34** | **−3.49** | **−3.54** | **−3.68** | **−3.69** | **−3.65** | −4.53 | **−4.50** | −4.71 | −4.67 | −4.96 | −4.87 | −5.15 | −5.35 |
| $b_{2g}$ $d_{xy}$ | −3.67 | −3.65 | −3.63 | −3.78 | −3.91 | −3.66 | **−4.52** | −4.50 | −4.68 | **−4.61** | −4.82 | −4.71 | −5.03 | −5.16 |
| $1a_{1u}$ | −3.83 | −3.85 | −3.82 | −3.94 | −3.95 | −3.83 | −4.58 | −4.54 | **−4.64** | −4.62 | **−4.60** | **−4.53** | **−4.78** | **−4.76** |
| $1a_{2u}$ | −5.03 | −4.69 | −4.86 | −4.99 | −5.23 | −4.57 | −5.95 | −5.88 | −6.03 | −5.29 | −5.78 | −5.54 | −5.98 | −6.13 |

[a]All MOs are in traditional $D_{4h}$ point group notation. For low-symmetry complexes, the average energies for nearly degenerate "$e_g$" MOs are shown in the table. The HOMO and LUMO MOs are shown in bold.

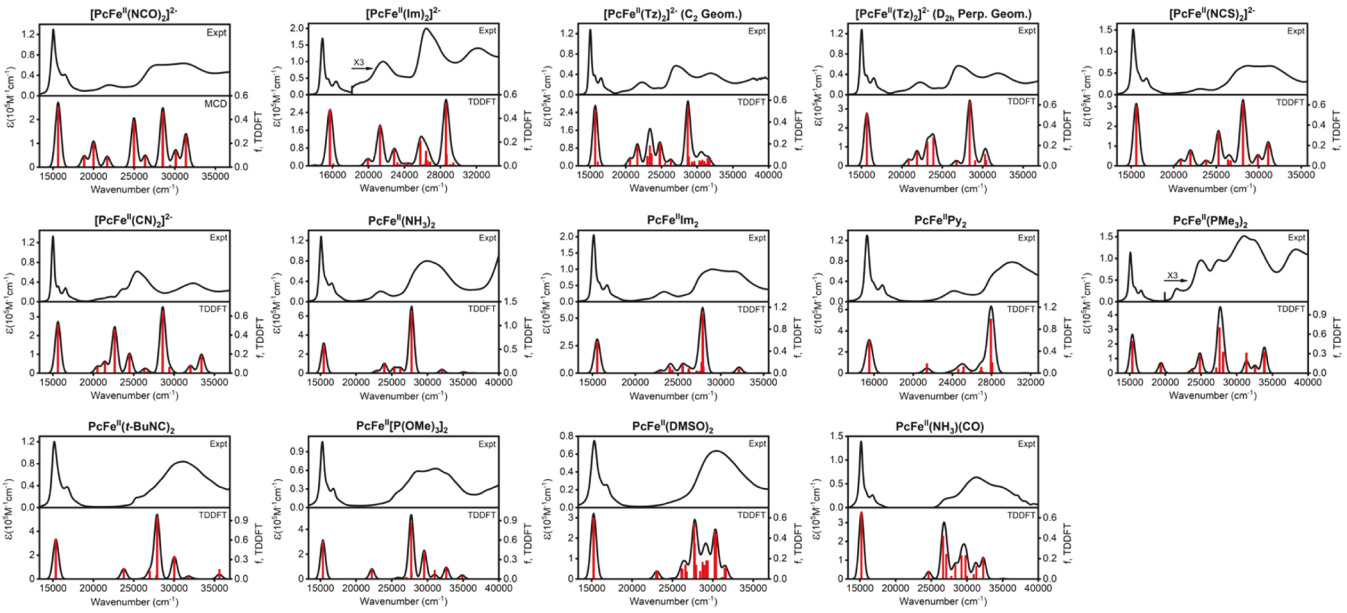


**Figure 7.** Experimental (top) and TDDFT-predicted (bottom) UV−vis spectra of the axially coordinated phthalocyanines using the MPWLYP exchange-correlation functional.

analyses. Moreover, in the case of the $PcFe(DMSO)_2$ and $PcFe(NH_3)(CO)$ complexes, the energy of the $MLCT_1$ band was also predicted to be higher than the $B_2$ and (in the case of the latter compound) N bands that are phthalocyanine-centered.

## DISCUSSION

Before the additive correlations between Lever's electrochemical $E_L$ scale[73,75] and the energy of the MLCT bands can be discussed, we need to accurately interpret the MCD and computational data for the $PcFeL_2$, PcFeL′L″, and $[PcFeX_2]^{2-}$ complexes. First, in our hands, the experimentally observed and TDDFT-predicted solvatochromic effect for the $[PcFeX_2]^{2-}$ complexes (X = $NCO^-$, $NCS^-$, and $CN^-$) in DCM, DMF, and DMSO is small. The $[PcFeX_2]^{2-}$ (X = $Im^-$ or $Tz^-$), $PcFeL_2$ (L = $PR_3$, *t*BuNC, $P(OBu)_3$, or DMSO), and $PcFe(n\text{BuNH}_2)(CO)$ complexes either have insufficient solubility in counterpart solvents or suffer from aggregation or low-stability problems in polar or nonpolar solvents and thus, solvatochromic effects cannot be measured for these compounds in an accurate way. $PcFeL_2$ (L = $NH_3$, $n\text{BuNH}_2$, and Im) have a moderate (~400−1300 $cm^{-1}$) solvatochromic effect for the MLCT band observed between 420 and 440 nm (Supporting Information Figure S4). Such a solvatochromic effect reflects the formation of the intermolecular hydrogen bond(s) between the axial ligand and the solvent molecules, and will be discussed in detail (on the basis of X-ray crystallographic data as well as NMR, and Mössbauer spectroscopies) in the follow-up paper. Thus for the analysis provided below, the only data collected by Stillman's[61,62] and our groups in DCM will be used for all compounds that are soluble and remain monomeric in this solvent. Since $Na_2[PcFeX_2]$ (X = $Im^-$ or $Tz^-$) complexes are not stable in DCM, we will present data obtained in DMF solutions.

Next, the DFT-predicted energies of the frontier MOs imply that the degenerate, *XY*-polarized MLCT transitions in $PcFeL_2$, PcFeL′L″, and $[PcFeX_2]^{2-}$ complexes can originate from $e_g$ (Fe, $d_\pi$) → $1b_{1u}$, $1b_{2u}$, $1a_{2u}$, and $1a_{1u}$ (Pc, $\pi^*$) single-electron transitions (in traditional $D_{4h}$ symmetry group notation, Figure 1). The bands that predominantly originate from the $e_g$ (Fe, $d_\pi$) → $1b_{1u}$ (Pc, $\pi^*$) and $e_g$ (Fe, $d_\pi$) → $1b_{2u}$ (Pc, $\pi^*$) single-electron transitions were labeled as $MLCT_1$ and $MLCT_2$, respectively, by Stillman's group.[61] The $MLCT_3$ band at ~27,000 $cm^{-1}$ that is dominated by the $e_g$ (Fe, $d_\pi$) → $1a_{2u}$ (Pc,


https://doi.org/10.1021/acs.inorgchem.2c00721
Inorg. Chem. 2022, 61, 8250−8266

**Table 2. Properties of the Selected Excited States Predicted by TDDFT Calculations Using MPWLYP Exchange-Correlation Functional**

| assign. | $E$/1000 ($cm^{-1}$) | wavelength (nm) | $f$ | contributions |
|---|---|---|---|---|
| | | | | $[PcFe(NCO)_2]^{2-}$ |
| Q[a] | 15.6 | 640 | 0.506 | 94% H-3 → L/L + 1, 2% H/H-1 → L + 2, 2% H-8 → L/L + 1 |
| $MLCT_1$[a] | 18.8 | 531 | 0.089 | 94% H/H-1 → L + 2, 4% H/H-1 → L + 3 |
| $MLCT_2$[a] | 20.0 | 500 | 0.202 | 93% H/H-1 → L + 3, 3% H-1/H → L + 2 |
| | | | | $[PcFe(Im^-)_2]^{2-}$ |
| Q | 15.7 | 637 | 0.457 | 82% H-3 → L/L + 1, 7% H-5 → L/L + 1 |
| $MLCT_1$ | 19.9 | 502 | 0.060 | 92% H/H-1 → L + 2, 4% H-6 → L/L + 1, 3% H-1 → L + 3 |
| $MLCT_2$ | 21.3 | 470 | 0.339 | 58% H/H-1 → L + 3, 27% H-6 → L/L + 1, 4% H-1 → L + 2, 2% H-10 → L/L + 1 |
| | | | | $[PcFe(1\text{-}Tz^-)_2]^{2-}$ |
| Q | 15.7 | 637 | 0.474 | 95% H-3 → L + 1/L, 2% H-6 → L/L + 1 |
| $MLCT_1$ | 20.6 | 486 | 0.065 | 94% H/H-1 → L + 2, 4% H-1/H → L + 3 |
| $MLCT_2$ | 21.6 | 463 | 0.182 | 87% H/H-1 → L + 3, 6% H-6 → L + 1/L, 3% H-1/H → L + 2 |
| | | | | $[PcFe(4\text{-}Tz^-)_2]^{2-}$ |
| Q[a] | 15.7 | 638 | 0.516 | 95% H-3 → L/L + 1, 2.18% H-8 → L + 1/L |
| $MLCT_1$[a] | 20.8 | 480 | 0.062 | 94% H/H-1 → L + 2, 4% H-1/H → L + 3 |
| $MLCT_2$[a] | 21.9 | 457 | 0.132 | 77% H/H-1 → L + 3, 10% H-8 → L + 1/L, 9% H-1/H → L + 7 |
| | | | | $[PcFe(NCS)_2]^{2-}$ |
| Q[a] | 15.6 | 641 | 0.587 | 95% H-3 → L + 1/L, 2% H-8 → L/L + 1 |
| $MLCT_1$[a] | 20.8 | 480 | 0.061 | 97% H/H-1 → L + 2 |
| $MLCT_2$[a] | 22.0 | 455 | 0.149 | 96% H-1/H → L + 3 |
| | | | | $[PcFe(CN)_2]^{2-}$ |
| Q[a] | 15.6 | 640 | 0.510 | 93% H-3 → L + 1/L, 4.86% H-4 → L/L + 1 |
| $B_1$[a] | 20.5 | 488 | 0.066 | 82% H-4 → L/L + 1, 12% H-1/H → L + 2, 2% H-3 → L + 1/L, 2% H/H-1 → L + 3 |
| $MLCT_1$[a] | 21.4 | 466 | 0.115 | 81% H/H-1 → L + 2, 10% H-1/H → L + 3, 7% H-4 → L + 1/L |
| $MLCT_2$[a] | 22.6 | 442 | 0.459 | 85% H/H-1 → L + 3, 6% H-1/H → L + 2, 4% H-4 → L/L + 1, 2% H-3 → L + 1/L |
| | | | | $PcFe(NH_3)_2$ |
| Q | 15.5 | 646 | 0.587 | 97% H-3 → L/L + 1 |
| $MLCT_1$ | 22.9 | 437 | 0.051 | 96% H-1/H-2 → L + 2 |
| $MLCT_2$ | 23,958 | 417 | 0.190 | 91% H-1/H-2 → L + 4, 5% H-4 → L/L + 1 |
| | | | | $PcFe(Im)_2$ |
| Q | 15.6 | 643 | 0.577 | 95% H-3 → L/L + 1 |
| $MLCT_1$ | 22.9 | 436 | 0.050 | 95% H/H-1 → L + 2 |
| $MLCT_2$ | 24.0 | 416 | 0.119 | 81% H/H-1 → L + 3, 8% H-5 → L/L + 1, 7% H-4 → L/L + 1 |
| | | | | $PcFePy_2$ |
| Q[a] | 15.5 | 645 | 0.586 | 97% H → L/L + 1 |
| $MLCT_1$[a] | 23.9 | 418 | 0.031 | 95% H-2/H-3 → L + 4, 3% H-3/H-2 → L + 5 |
| $MLCT_2$[a] | 24.6 | 406 | 0.074 | 84% H-3/H-2 → L + 5, 9% H-4 → L/L + 1, 4% H-5 → L + 1/L |
| | | | | $PcFe(PMe_3)_2$ |
| Q | 15.4 | 651 | 0.495 | 93% H-1 → L/L + 1, 6% H-4 → L + 1/L |
| L + $B_1$ | 19.4 | 516 | 0.134 | 92% H-4 → L/L + 1, 5% H-1 → L + 1/L |
| $MLCT_1$ | 23.8 | 420 | 0.052 | 94% H-2/H-3 → L + 2, 4% H-3/H-2 → L + 3 |
| $MLCT_2$ | 24.8 | 403 | 0.264 | 89% H-2/H-3 → L + 3, 5% H-6 → L + 1/L, 4% H-3/H-2 → L + 2 |



https://doi.org/10.1021/acs.inorgchem.2c00721
Inorg. Chem. 2022, 61, 8250−8266

**Table 2. continued**

| assign. | $E$/1000 ($cm^{-1}$) | wavelength (nm) | $f$ | contributions |
|---|---|---|---|---|
| | | | | PcFe(tBuNC)$_2$ |
| Q | 15.4 | 651 | 0.620 | 96% H → L/L + 1, 3% H-4 → L + 1/L |
| $B_1$ | 23.8 | 421 | 0.160 | 84% H-4 → L/L + 1, 6% H-6 → L/L + 1, 4% H-5 → L + 1/L |
| $MLCT_1$ | 26.2 | 382 | 0.006 | 86% H-2/H-3 → L + 2, 7% H-6 → L + 1/L, 4% H-3/H-2 → L + 2, 3% H-6 → L/L + 1 |
| $MLCT_2$ | 27.0 | 371 | 0.126 | 38% H-2/H-3 → L + 3, 34% H-6 → L/L + 1, 16% H-9 → L/L + 1, 4% H-3/H-2 → L + 2, 3% H-5 → L + 1/L |
| $MLCT_2$ | 27.9 | 358 | 0.955 | 54% H-2/H-3 → L + 3, 32% H-6 → L/L + 1, 4% H-3/H-2 → L + 2, 3% H-4 → L/L + 1 |
| | | | | PcFe[P(OMe)$_3$]$_2$ |
| Q | 15.4 | 651 | 0.581 | 94% H → L/L + 1, 3% H-4 → L + 1/L |
| $B_1$ + L | 22.2 | 450 | 0.152 | 92% H-4 → L/L + 1, 2% H-6 → L/L + 1, 2% H → L + 1/L |
| $MLCT_1$ | 26.0 | 385 | 0.017 | 85% H-2/H-3 → L + 3, 8% H-6 → L/L + 1, 6% H-5 → L/L + 1 |
| $MLCT_2$ | 26.7 | 374 | 0.003 | 66% H-2/H-3 → L + 4, 20% H-6 → L + 1/L, 4% H-9 → L/L + 1, 3% H → L + 6/L + 7, 3% H-5 → L + 1/L |
| | | | | PcFe(DMSO)$_2$ |
| Q | 15.2 | 657 | 0.597 | 98% H → L/L + 1 |
| L + $B_1$ | 23.0 | 435 | 0.080 | 88% H-4 → L/L + 1, 3% H-4 → L + 1/L, 2% H-6 → L/L + 1 |
| $B_2$ | 26.2 | 383 | 0.106 | 45% H-6 → L/L + 1, 23% H-2/H-3 → L + 3, 17% H-6 → L + 1/L, 5% H-9 → L/L + 1, 3% H-3/H-2 → L + 4 |
| $MLCT_1$ | 26.7 | 376 | 0.141 | 66% H-2/H-3 → L + 3, 14% H-9 → L/L + 1, 9% H-3/H-2 → L + 4, 5% H-6 → L/L + 1 |
| $MLCT_2$ | 27.7 | 361 | 0.538 | 74% H-2/H-3 → L + 4, 6% H-3/H-2 → L + 3, 4% H-6 → L + 1/L, 3% H-9 → L + 1/L, 3% H-12 → L + 1/L |
| | | | | PcFe($NH_3$)(CO) |
| Q | 15.2 | 657 | 0.661 | 97% H → L/L + 1 |
| $B_1$ | 24.6 | 406 | 0.073 | 54% H-4 → L/L + 1, 36% H-5 → L/L + 1, 7% H-6 → L/L + 1 |
| N | 26.7 | 375 | 0.419 | 66% H-9 → L/L + 1, 18% H-6 → L + 1/L, 4% H-4 → L + 1/L, 3% H-3/H-2 → L + 3, 2% H → L + 5/L + 6 |
| $B_2$ | 27.1 | 369 | 0.244 | 39% H-6 → L + 1/L, 22% H-9 → L/L + 1, 17% H-4 → L + 1/L, 7% H → L + 5/L + 6, 3% H-15 → L/L + 1, 3% H-2/H-3 → L + 2, 3% H-5 → L + 1/L |
| $MLCT_1$ | 28.4 | 352 | 0.142 | 91% H-2/H-3 → L + 2, 3% H-3/H-2 → L + 4, 2% H-6 → L + 1/L |
| $MLCT_2$ | 29.3 | 342 | 0.230 | 49% H-2/H-3 → L + 4, 23% H-1 → L + 6/L + 5, 13% H-2/H-3 → L + 7, 9% H-1 → L + 9/L + 10 |

[a]Degenerate state, for all other states, average values are used; in all cases, Q-band is dominated by the "$a_{1u}$" → $e_g$, $B_1$-band is dominated by the "$a_{2u}$" → $e_g$, L + $B_1$-band is dominated by the "$L_{ax}$ + $a_{2u}$" → $e_g$, $MLCT_1$ is dominated by the "$d_\pi$" → "$b_{1u}$", and $MLCT_2$ is dominated by the $d_\pi$ → "$b_{2u}$" single-electron excitations.



https://doi.org/10.1021/acs.inorgchem.2c00721
Inorg. Chem. 2022, 61, 8250−8266

$\pi^*$) single-electron transition was predicted by Sumimoto and co-authors[113] for the $[PcFe(CN)_2]^{2-}$ complex on the basis of TDDFT (B3LYP/6-31G(d)) calculations. The $MLCT_4$ band energy ($e_g$ (Fe, $d_\pi$) → $1a_{1u}$ (Pc, $\pi^*$)) has not been discussed in the literature. Stillman and Ough used a 2050 $cm^{-1}$ energy difference for the $e_g$ (Fe, $d_\pi$) → $1b_{1u}$ (Pc, $\pi^*$) and $e_g$ (Fe, $d_\pi$) → $1b_{2u}$ (Pc, $\pi^*$) single-electron transitions as a starting point for their MCD spectral analysis of $PcFeL_2$, PcFeL′L″, and $[PcFeX_2]^{2-}$ complexes (Figure 1). This energy difference originates from the MCD data analysis of the $[Pc(-3)Mg]^{-\bullet}$ anion-radical complex conducted by Stillman and co-workers.[114] The discrepancy between this value (2050 $cm^{-1}$) and, proposed on the basis of MCD and UV−vis spectral analysis, the $MLCT_1$−$MLCT_2$ energy gap for $[PcFe(CN)_2]^{2-}$ (∼7900 $cm^{-1}$), $PcFe(NH_3)_2$ (∼4300 $cm^{-1}$), and $PcFe(NH_3)(CO)$ (∼1200 $cm^{-1}$) was attributed to configuration interaction (CI) and the presence of the 3d electrons in the iron compounds.[61] Again, this assumption was a very reasonable starting point taking into consideration the lack of TDDFT calculations available for these systems in 1994. Our DFT calculations using three exchange-correlation functionals (MPWLYP, O3LYP, and TPSSh) as well as the DFT calculations reported by Sumimoto and co-workers[113] using the B3LYP exchange-correlation functional suggest that the energy difference between the $1b_{1u}$ and $1b_{2u}$ MOs is quite small (0.13−0.16 eV). Unlike LUMO and LUMO + 1 (Pc-centered MOs of $e_g$ symmetry) that have a substantial contribution from the iron d-orbitals, the $1b_{1u}$, $1b_{2u}$, and $1a_{2u}$ virtual MOs cannot be mixed with the metal-centered d-orbitals, although the $1a_{2u}$ orbital can mix with the axial ligand orbitals (Figure 1). As a consequence, one might expect that the DFT-predicted energies of the LUMO and LUMO + 1 MOs will have a significant dependency on the exchange-correlation functional (and specifically the amount of the exact Hartree−Fock exchange present in the functional) used for the calculations, while such dependency should be smaller for the $1b_{1u}$, $1b_{2u}$, and $1a_{2u}$ virtual MOs. Indeed, when the DFT-predicted energy differences between the $1e_g$ and $1b_{1u}$, $1b_{1u}$ and $1b_{2u}$, and $1b_{2u}$ and $1a_{2u}$ MOs are plotted against the amount of exact Hartree−Fock exchange in the functional, it became clear that the above-mentioned argument is correct. For instance, for the $[PcFe(CN)_2]^{2-}$ complex, the energy difference between the $1e_g$ and $1b_{1u}$ MOs has a clear functional dependence and varies between 1.09 and 1.72 eV for functionals with 0−54% of Hartree−Fock exchange. On the other hand, it only varies between 0.12 and 0.24 eV for the energy gap between the $1b_{1u}$ and $1b_{2u}$ MOs, while it is nearly constant for the energy difference predicted between the $1b_{2u}$ and $1a_{2u}$ MOs (Supporting Information Figure S5). Even when the traditional Hartree−Fock calculations for this compound are considered, the $1b_{1u}$−$1b_{2u}$ energy gap remains small (0.34 eV). In addition to a small functional dependency, the DFT-predicted $1b_{1u}$−$1b_{2u}$ energy gap is nearly constant for a given exchange-correlation functional across the $E_L$ axis (Supporting Information Figure S5), which (ignoring configurational interactions) implies nearly constant $MLCT_1$−$MLCT_2$ energy gaps in all of the compounds of interest. Our TDDFT calculations with the MPWLYP, O3LYP, and TPSSh functionals predict a 800−1450 $cm^{-1}$ energy gap between the $MLCT_1$ and $MLCT_2$ states in the $PcFeL_2$, PcFeL′L″, and $[PcFeX_2]^{2-}$ complexes, which also correlates well with the 1290 $cm^{-1}$ predicted by Sumimoto and co-authors[113] for the $[PcFe(CN)_2]^{2-}$ compound and Stillman's estimate of 2050 $cm^{-1}$ gained from the spectroscopy of the $[Pc(-3)Mg]^{-\bullet}$ anion-radical.[114] A small $1b_{1u}$−$1b_{2u}$ energy gap leads to the following interesting question. The MCD spectra of the $[PcFeX_2]^{2-}$ (X = $NCO^-$, $Im^-$, $Tz^-$, and $NCS^-$) and $PcFeL_2$ (L = $NH_3$, Im, $n$BuNH$_2$, and Py) compounds, in which the 400−450 nm MLCT region is well separated, are represented by an asymmetric dispersion curve in which the visible MCD $A$-term is located at a higher energy and an additional signal with negative amplitude is located at a lower energy (Figure 3). The energy difference between the negative component of the visible $A$-term and lower-energy visible $B$-term is close to 800 $cm^{-1}$ in all cases. Similarly, the absorption spectra of these complexes in the same spectral envelope have a visible shoulder in the lower-energy side. Again, the energy difference between the shoulder and the main band is about 800 $cm^{-1}$. In their analysis reported in 1994, Stillman and Ough deconvoluted the MCD spectra of $PcFeL_2$ (L = $NH_3$, Py, Im, 1-MeIm, 4-MePy, and Pip) in this region using one MCD $A$-term and one MCD $B$-term of negative amplitude.[61] The nature of this $B$-term has not been discussed in the literature; however, one might argue that it can originate from a $Z$-polarized $b_{2g}$ (Fe, $d_{xy}$) → $1b_{1u}$ (Pc, $\pi^*$) transition mentioned by Stillman and Ough. In this case, using a simplistic single-electron approximation, the energy of the $d_{xy}$ orbital should be higher than that of the $d_\pi$ orbitals and a $B$-term is expected in the MCD spectrum (Supporting Information Figure S6). Alternatively, the low-energy signal of negative amplitude can originate from the MCD $A$-term that is closely spaced near the visible $A$-term. In this case, two MCD $A$-terms will represent two closely spaced $MLCT_1$ and $MLCT_2$ excited states (Supporting Information Figure S6). Our TDDFT calculations using three different exchange-correlation functionals suggest that the oscillator strength for the $b_{2g}$ (Fe, $d_{xy}$) → $1b_{1u}$ (Pc, $\pi^*$) transition is very small ($f$ = 0−0.002) compared to the predicted oscillator strength of the $MLCT_1$ transition ($f$ = 0.006−0.14), which does not support the assignment of these low-energy shoulders as $b_{2g}$ (Fe, $d_{xy}$) → $1b_{1u}$ (Pc, $\pi^*$) in nature. Moreover, TDDFT predicts that in the $[PcFeX_2]^{2-}$ (X = $NCO^-$, $Im^-$, $Tz^-$, and $NCS^-$) complexes, the energy of the $b_{2g}$ (Fe, $d_{xy}$) → $1b_{1u}$ (Pc, $\pi^*$) transition should be higher in energy compared to the $MLCT_1$ (Supporting Information Table S2). This also agrees well with the MCD spectra assignments of the highly deformed $Pc^{Ph8}FcPy_2$ complex provided by Kobayashi and Fukuda.[115] Indeed, these authors have shown that the MLCT transition originating from the $d_{xy}$ orbital has a higher energy compared to the MLCT transition that originates from the $d_\pi$ MOs.

Finally, the relative energies of the $MLCT_1$ and $MLCT_2$ transitions with respect to $\pi \rightarrow \pi^*$ transitions originating from the phthalocyanine core should be considered. Historically, it was always assumed that the first higher energy (after the Q-band) MCD $A$-term is associated with the $MLCT_1$ transition.[61,62] However, a previous report by Sumimoto and co-authors[113] as well as our TDDFT calculation suggest that this is not always the case. For instance, TDDFT calculations predict that the $B_1$ (predominantly $1a_{2u}$ (Pc + L, $\pi$) → $1e_g$ (Pc, $\pi^*$) single-electron transition) band should have a lower energy than $MLCT_1$ in the $[PcFe(CN)_2]^{2-}$, $PcFe(PMe_3)_2$, $PcFe(t$BuNC$)_2$, and $PcFe[P(OMe_3)]_2$ complexes (Supporting Information Table S2). The $B_1$ band has $XY$ polarization and is expected to have an MCD $A$-term shape. As discussed above, the $1a_{2u}$ orbital can mix with the axial ligands, and thus, its energy has a tendency to fluctuate significantly. As a


https://doi.org/10.1021/acs.inorgchem.2c00721
Inorg. Chem. 2022, 61, 8250−8266

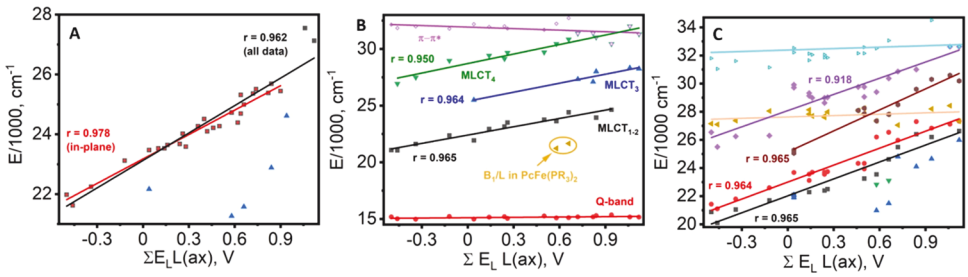


**Figure 8.** Correlation between $\Sigma E_L$ L(ax) and the experimental MLCT band position in the UV−vis spectra (A); $\Sigma E_L$ L(ax) and the experimental crossing point for the visible MCD *A*-terms (B); and $\Sigma E_L$ L(ax) and the experimental energies of the MCD *A*-terms from the deconvolution analysis (C). According to TDDFT calculations, blue triangles correspond to $B_1$ (predominantly $1a_{2u} \rightarrow 1e_g^*$) $\pi-\pi^*$ transitions that have no linear dependency on $\Sigma E_L$ L(ax) values.

**Table 3. MCD *A*-Term Centers for the Degenerate Transitions in the $PcFeL_2$, PcFeL′L″, and $[PcFeX_2]^{2-}$ Complexes in the Charge-Transfer Region**[a]

| compound | band center (nm) | | | | | | | | | | ref |
|---|---|---|---|---|---|---|---|---|---|---|---|
| $[PcFe(NCO)_2]^{2-}$ | 479 | 465 | 377 | 368 | 314 | | | | | | tw |
| $[PcFe(Im)_2]^{2-}$ | 498 | 475 | 392 | 369 | 322 | 319 | | | | | tw |
| $[PcFe(Tz)_2]^{2-}$ | 475 | 459 | 381 | 366 | 316 | 313 | | | | | tw |
| $[PcFe(NCS)_2]^{2-}$ | 461 | 442 | 372 | 357 | 321 | | | | | | tw |
| $[PcFe(CN)_2]^{2-}$ | 456 | 422 | 399 | 337 | | | | | | | tw |
| $[PcFe(CN)_2]^{2-}$ | 453 | | 396 | 334 | 307 | 279 | 251 | | | | 61 |
| $PcFe(NH_3)_2$ | 449 | 433 | 355 | 343 | 311 | | | | | | tw |
| $PcFe(NH_3)_2$ | | 424 | 359 | 341 | 316 | 273 | 253 | | | | 61 |
| $PcFe(MeIm)_2$ | | 422 | 361 | 345 | 312 | 271 | 248 | | | | 61 |
| $PcFeIm_2$ | 446 | 425 | 362 | 349 | 314 | 273 | | | | | tw |
| $PcFeIm_2$ | | 422 | 361 | 345 | 312 | 270 | 248 | | | | 61 |
| $PcFe(n\text{BuNH}_2)_2$ | 444 | 421 | 357 | 345 | 314 | 277 | | | | | tw |
| $PcFe(MePy)_2$ | | 411 | 356 | 336 | 311 | 277 | | | | | 61 |
| $PcFePy_2$ | 430 | 418 | 359 | 344 | 337 | 307 | | | | | tw |
| $PcFePy_2$ | | 411 | 354 | 336 | 311 | 277 | | | | | 61 |
| $PcFe(PBu_3)_2$ | 477 | 438 | 425 | 382 | 366 | 340 | 308 | 266 | 257 | 249 | tw |
| $PcFe(PMe_3)_2$ | 465 | 433 | 406 | 375 | 360 | 329 | 302 | 262 | | | tw |
| $PcFe(t\text{BuNC})_2$ | 403 | 392 | 385 | 370 | 351 | 333 | | | | | tw |
| $PcFe[P(OBu)_3]_2$ | 415 | 379 | 366 | 338 | 323 | 251 | | | | | tw |
| $PcFe(DMSO)_2$ | 406 | 382 | 373 | 355 | 330 | 290 | | | | | tw |
| $PcFe(NH_3)(CO)$ | | 369 | 352 | 327 | 307 | 278 | | | | | 61 |
| $PcFe(n\text{BuNH}_2)(CO)$ | 385 | 376 | 366 | 331 | 307 | 279 | | | | | tw |

[a]tw = this work.

consequence, the TDDFT-predicted energy of the $B_1$ band deviates significantly from the nature of the axial ligands. In the case of the $PcFe(DMSO)_2$ and $PcFe(NH_3)(CO)$ complexes, TDDFT calculations predict several phthalocyanine-centered degenerate $\pi-\pi^*$ excited states with energies lower than the $MLCT_1$ transition (Supporting Information, Table S2). Thus, extra care should be taken for the accurate assignments of the charge-transfer bands in the $PcFeL_2$, PcFeL′L″, and $[PcFeX_2]^{2-}$ complexes.

When raw data for the most intense low-energy UV−vis peaks in region II for the $PcFeL_2$, PcFeL′L″, and $[PcFeX_2]^{2-}$ complexes are plotted against the $\Sigma E_L$ L(ax) values to probe the validity of eq 4 (Figure 8A), one can see five clear outliers coded as blue triangles. These UV−vis bands are associated with the lowest energy (after the Q-band) MCD *A*-term and, according to the TDDFT calculations, should be assigned as $B_1$ ($1a_{2u}$ (Pc + L, $\pi$) → $1e_g$ (Pc, $\pi^*$)) phthalocyanine-centered transitions. Once these points are removed from the correlation, the correlation coefficient for the linear regression was 0.962 for all data points or 0.978 for the points in which the central iron ion is located in the plane of the phthalocyanine ligand.

As MCD spectroscopy tends to provide a complimentary resolution of the UV−vis data, we plotted the *Y*-axis crossing points for the visible *A*-terms observed in the MCD spectra of the $PcFeL_2$, PcFeL′L″, and $[PcFeX_2]^{2-}$ complexes against the $\Sigma E_L$ L(ax) values (Figure 8B). It is obvious that the use of the energies of crossing points in the correlation analysis is quite approximate; however, even with such a crude approximation, several trends can be clearly seen. First, the energy of the MCD *A*-term which corresponds to the Q-band at ∼15,000 $cm^{-1}$ is independent of the $\Sigma E_L$ L(ax) values. This is expected as Q-band in phthalocyanines is an almost pure $1a_{1u}$ (Pc, $\pi$) → $1e_g$ (Pc, $\pi^*$) ligand-centered transition. Next, a unique MCD *A*-term at a low energy was observed in the case of the $PcFe(PR_3)_2$ complexes. According to TDDFT calculations, this *A*-term represents the $B_1$ band, which is dominated by a $1a_{2u}$ (Pc + L, $\pi$) → $1e_g$ (Pc, $\pi^*$) single-electron contribution. The energy of the $1a_{2u}$ orbital in $PcFe(PR_3)_2$ is highly destabilized because of the large contribution from the lone


https://doi.org/10.1021/acs.inorgchem.2c00721
Inorg. Chem. 2022, 61, 8250−8266

pair from two phosphine axial ligands. Next, three nearly parallel correlation lines that have clear axial dependency have been observed (Figure 8B). All three lines have nearly identical slopes and are separated by 3000−3300 $cm^{-1}$ from each other. We label these correlations as $MLCT_{1-2}$, $MLCT_3$, and $MLCT_4$ in Figure 8B. The rationale for combining the $MLCT_1$ and $MLCT_2$ transitions under the same curve is that TDDFT data from Sumimoto's[113] and our work are suggestive of the $MLCT_1$−$MLCT_2$ gap in the 725−1700 $cm^{-1}$ range (with the majority of those predicted at ∼1200 $cm^{-1}$), which is not easy to clearly resolve in the MCD spectra as discussed above. The TDDFT-predicted energies of $MLCT_3$ and $MLCT_4$, on the other hand, are better separated from the energies of $MLCT_1$ and $MLCT_2$ (see discussion below). Obviously, this assumption should be treated with caution and is the main reason why we have deconvoluted the MCD spectra of $PcFeL_2$, PcFeL′L″, and $[PcFeX_2]^{2-}$ complexes in two different ways. Another important observation from Figure 8B is that the energies of the $MLCT_4$ bands for complexes with high $\Sigma E_L$ L(ax) values coalesce with the energies of the phthalocyanine-centered $\pi-\pi^*$ transitions observed at ∼31,000 $cm^{-1}$. The latter transition is also almost independent of the nature of the axial ligands, which is a reason for the confident assignment of the last correlation line for the phthalocyanine-centered $\pi-\pi^*$ transition. Finally, the correlation results for the $[PcFe(CN)_2]^{2-}$ complex imply that the energy of the $B_1$ and $MLCT_1$ bands should be close to each other, which agrees well with our TDDFT calculations.

Of course, the use of the crossing point of the visible MCD *A*-terms in the correlation analysis is not the best approach in providing a complete picture on the electronic structure and nature of the excited states in $PcFeL_2$, PcFeL′L″, and $[PcFeX_2]^{2-}$ complexes because some of the overlapping *A*-terms can visibly appear as a sum of MCD *B*- and *A*-terms (see Supporting Information Figure S6 as an example). This is a situation observed for the transitions in $PcFeL_2$, PcFeL′L″, and $[PcFeX_2]^{2-}$ complexes in the B-band region where a large number of bands are closely spaced in energy and heavily overlap. In this case, as introduced by Stillman and co-workers for phthalocyanines,[61] simultaneous band deconvolution analysis of UV−vis and MCD spectra is the best alternative for more accurate analysis of the excited states. Since TDDFT predicts that the energy gap between $MLCT_1$ and $MLCT_2$ is rather small, we attempted to accommodate this observation in our analyses (Figure 4B); however, we also conducted a more traditional deconvolution analysis, similar to that done by Stillman and co-workers in 1994 (Figure 4A).[61] As one can see from Figure 4, in the former case, two (closely spaced in energy) *A*-terms were considered in the first MLCT region, while in the latter case, the same region was deconvoluted with a single *A*-term. The energies of the *A*-terms predicted by the deconvolution analysis again correlate well with the $\Sigma E_L$ L(ax) values (Figure 8C and Table 3). There are several *A*-terms that were observed with energies that are nearly independent of the nature of the axial ligands. These can be assigned as phthalocyanine-centered excited states. The MLCT transition, on the other hand, has clear axial ligand dependency and correlation coefficients close to those observed with the MCD *A*-terms crossing points.

The plot of the energies of the MLCT transitions predicted by TDDFT calculations versus $\Sigma E_L$ L(ax) values is shown in Figure 9A. The correlation coefficients for the TDDFT-predicted $MLCT_{1-3}$ transitions are close to those seen in the

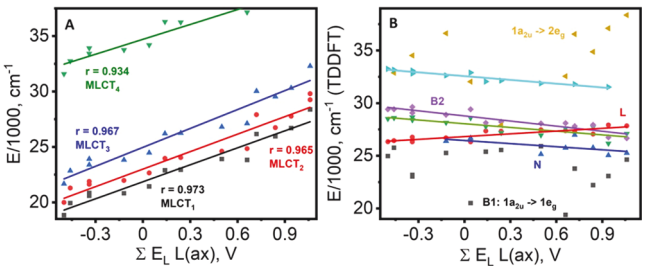


**Figure 9.** Correlation between $\Sigma E_L$ L(ax) and the TDDFT-predicted MLCT band energies (A; black squares represent data for $MLCT_1$, red circles for $MLCT_2$, blue triangles for $MLCT_3$, and green triangles for $MLCT_4$ transitions); $\Sigma E_L$ L(ax) and the TDDFT-predicted $\pi-\pi^*$ transitions (B; black squares and gold triangles represent excited states that are dominated by the $\pi-\pi^*$ from $1a_{2u}$ MO, blue triangles represent N-band, red circles for L band, and magenta rhombs for B2 band). For numerical values, see the Supporting Information and Table 2.

MCD plots (Figure 8B) and their slopes are close to the slopes observed for the fitted MCD data. One visible discrepancy between the TDDFT calculations and the MCD-based position of its *A*-terms that have a prominent axial ligand dependency is the energy intervals for the MLCT bands. The TDDFT calculations predict that $MLCT_{1-3}$ in the $PcFeL_2$, PcFeL′L″, and $[PcFeX_2]^{2-}$ complexes are separated by ∼1000 ($MLCT_{1-2}$) and ∼2000 ($MLCT_{2-3}$) $cm^{-1}$ (Figure 8), which correlates very well with the respective separation of ∼1000 and ∼3000 $cm^{-1}$ predicted by band deconvolution analysis and the ∼3000 $cm^{-1}$ interval observed between the first (second for $PcFe(PR_3)_2$ complexes) and second visible *A*-terms in the experimental spectra of these compounds (Figure 3). However, for most of the compounds, it is difficult to derive the experimental position of $MLCT_3$ from the UV−vis and MCD spectra because it heavily overlaps with the other transitions, making the proposed assignment quite speculative. In addition, the TDDFT-predicted energy interval between the $MLCT_3$ and $MLCT_4$ bands is ∼10,000 $cm^{-1}$, while ∼3000 $cm^{-1}$ is expected from the MCD band deconvolution analysis. Yet, the TDDFT-predicted energies of the $MLCT_{1-3}$ transitions are well within expectation for TDDFT calculations, being ∼2000 $cm^{-1}$ in error. They are also lower than the typical errors for the energies of the MLCT transitions in ruthenium(II) and iron(II) complexes predicted by earlier Lever using eq 2, ∼2400 $cm^{-1}$.[77] The linear correlations shown in Figure 8A,B allow one to predict the expected position of the $MLCT_2$ band in the UV−vis and MCD spectra of $PcFeL_2$, PcFeL′L″, and $[PcFeX_2]^{2-}$ complexes. Equation 5 can be used to predict the $MLCT_2$ band in the UV−vis spectra (which correlates with the low-energy MLCT band maximum), while eq 6 can be used to predict the energy of the MCD *A*-term (which corresponds to the $MLCT_2$ band center) as long as $\Sigma E_L$ L(ax) values for the axial ligands are known. Based on our experimental data and TDDFT calculations, the energy of the $MLCT_1$ band then can be estimated as $E_{MLCT1}$ ($cm^{-1}$) = $E_{MLCT2}$ − 800 for both UV−vis and MCD spectra.

$$E_{MLCT2}(\text{UV} - \text{vis}, \text{cm}^{-1}) = 2720 \sum E_L L(\text{ax}) + 23174 \quad (5)$$

$$E_{MLCT2}(\text{MCD}, \text{cm}^{-1}) = 2444 \sum E_L L(\text{ax}) + 22402 \quad (6)$$



https://doi.org/10.1021/acs.inorgchem.2c00721
Inorg. Chem. 2022, 61, 8250−8266

The MLCT (Fe → Pc) transitions are not the only charge-transfer transitions that are expected in the UV−vis and MCD spectra of the $PcFeL_2$, PcFeL′L″, and $[PcFeX_2]^{2-}$ complexes. As was correctly pointed out by Stilman and Ough,[61] two symmetry allowed LMCT (ligand-to-metal charge transfer) transitions of Pc → Fe character are expected for these compounds in idealized $D_{4h}$ symmetry (Figure 1). These are dominated by the $1a_{2u}$ (Pc, $\pi$) → $a_{1g}$ (Fe, $d_{z^2}$) and $1b_{2u}$ (Pc, $\pi$) → $b_{1g}$ (Fe, $d_{x^2-y^2}$) single-electron transitions and are labeled as $LMCT_{Pc1}$ and $LMCT_{Pc2}$ in Figure 1, respectively. Both of these should result in MCD *B*-terms. The $LMCT_{Pc1}$ transitions were predicted between 31,000 and 36,700 $cm^{-1}$ from the TDDFT calculations using the MPWLYP functional. The predicted intensity of this excited state for the axial ligands with $\Sigma E_L$ L(ax) ≤ 0.5 is rather small, but it is substantial ($f > 0.1$) for the rest of the tested compounds. The $LMCT_{Pc2}$ transition was not found in the TDDFT calculations within the 120 lowest-energy states and, presumably, appears at higher energy. Next, the electronic structure of the axial ligands should be considered. DFT calculations predict that the negatively charged axial ligands with significant $\sigma$- and $\pi$-donating properties ($NCO^-$, $Im^-$, $Tz^-$, and $NCS^-$) should have axial ligand-centered $e_g$ and $e_u$ symmetry orbitals in the HOMO to HOMO − 10 region (Supporting Information Table S1). Excited states that are dominated by $e_g$ ($X^-$, $\pi$) → $1b_{1u}$, $1b_{2u}$, $1a_{2u}$, and $1a_{1u}$ (Pc, $\pi^*$) single-electron transitions can give rise of four interligand ILCT ($X^-$ → Pc) transitions with MCD *A*-term character that are labeled as $ILCT_{1\text{-}4}$ in Figure 1. The energies of $ILCT_1$, $ILCT_2$, and $ILCT_3$ were predicted (MPWLYP functional) between 23,300−30,100, 24,500−31,400, and 26,300−33,000 $cm^{-1}$, respectively. Excited states that are dominated by the $e_u$ ($X^-$, $\pi$) → $1e_g$ and $2e_g$ (Pc, $\pi^*$) single-electron transitions can give rise to two ILCT ($X^-$ → Pc) transitions with MCD *B*-term character that are labeled as $ILCT_{5-6}$ in Figure 1. The energies of $ILCT_5$ and $ILCT_6$ were predicted (MPWLYP functional) between 26,400 and 32,400 $cm^{-1}$. Finally, the excited state that is dominated by the $e_u$ ($X^-$, $\pi$) → $a_{1g}$ and $b_{1g}$ (Fe, $d_{z^2}$ and $d_{x^2-y^2}$) single-electron transitions can give rise to two LMCT ($X^-$ or L → Fe) transitions with MCD *A*-term character that are labeled as $LMCT_{L1-2}$ in Figure 1. The energy of $LMCT_{L1}$ was predicted (MPWLYP functional) between 28,900 and 36,700 $cm^{-1}$, while the energy of the $LMCT_{L2}$ state lies outside of the 120 lowest-energy excited states. The increase of the $\pi$-accepting character of the cyanide axial ligand results in the stabilization of the occupied, axial ligand-centered $e_g$ and $e_u$ MOs. As a result, the TDDFT-predicted energies of the $ILCT_{1-3}$ bands increased to 35,900−38,800 $cm^{-1}$. The $PcFeL_2$ and PcFeL′L″ complexes in which the axial ligand has a significant $\pi$-accepting character (Py, *t*BuNC, and $NH_3$/CO) have unoccupied, axial ligand-centered orbitals of *e* character that is reflective of the lowering of their molecular symmetries from the effective $D_{4h}$ to $D_{2d}$, $C_s$, and $C_i$ (even the symmetry of the $PcFe(tBuNC)_2$ and $PcFe(NH_3)$-(CO) complexes is $C_i$ or $C_s$ and the axial ligand's MOs that have $e_g$ or $e_u$ symmetries in $D_{4h}$ point group are still nearly degenerate and will be considered below as "*e*" symmetry orbitals). No degenerate or nearly degenerate unoccupied MOs in the LUMO to LUMO + 10 energy region were predicted for the $PcFeL_2$ (L = Im, $PMe_3$, and DMSO) complexes. Similar to the TDDFT calculations of Sumimoto and co-workers,[113] our TDDFT calculations on $PcFePy_2$ are indicative of *XY*-polarized (Pc → Py) transitions that originate from $1a_{1u}$, $1a_{2u}$, and $1b_{2u}$ (Pc, $\pi$) → "*e*" (Py, $\pi^*$) single-electron excitations and one *Z*-polarized transition dominated by the $1e_g$ (Pc, $\pi$) → "*e*" (Py, $\pi^*$) single-electron excitation (here we use $D_{4h}$ point group notation for the phthalocyanine and metal-centered orbitals to be consistent with the previous discussion and Figure 1). These transitions are labeled as $ILCT_{Pc1-4}$ in Figure 1 and were predicted at 20,100, 32,000, 33,000, and 34,900 $cm^{-1}$, respectively. In addition, two MLCT (Fe → Py) transitions labeled as $MLCT_{Fe1-2}$ in Figure 1 that originate from $e_g$ (Fe, $d_\pi$) → "*e*" (Py, $\pi^*$) and $b_{2g}$ (Fe, $d_{xy}$) → "*e*" (Py, $\pi^*$) single-electron transitions have *Z*- and *XY*-polarizations, respectively. According to TDDFT calculations, both of these transitions have small intensities. No Pc → *t*BuNC ILCT transitions were predicted by TDDFT calculations within the lowest-energy 120 excited states; however, $MLCT_{Fe1-2}$ transitions were predicted at 35,600 ($f = 0.15$) and 32,600 ($f = 0.004$) $cm^{-1}$. Finally, the $ILCT_{Pc1}$ transition was predicted at 30,000 $cm^{-1}$ with reasonable intensity ($f = 0.03$) for the $PcFe(NH_3)(CO)$ complex, while $MLCT_{Fe1-2}$ transitions in the 33,300−34,800 $cm^{-1}$ window were predicted to have zero intensities. Overall, our TDDFT calculations indicate that the axial ligands can contribute to the UV−vis and MCD spectra of $PcFeL_2$ and PcFeL′L″ complexes via MLCT, ILCT, and LMCT mechanisms.

## CONCLUSIONS

The position of the experimentally observed (in the UV−vis and MCD spectra) low-energy metal-to-ligand charge-transfer (MLCT) band in low-spin iron(II) phthalocyanine complexes of general formula $PcFeL_2$, PcFeL′L″, and $[PcFeX_2]^{2-}$ (L, L′, or L″ are neutral and $X^-$ is an anionic axial ligand) was correlated with the Lever's electrochemical $E_L$ scale values for the axial ligands. The TDDFT-predicted UV−vis spectra are in very good agreement with the experimental data for all complexes. In the majority of compounds, TDDFT predicts that the first degenerate MLCT band that correlates with the MCD *A*-term observed between 360 and 480 nm is dominated by an $e_g$ (Fe, $d_\pi$) → $b_{1u}$ (Pc, $\pi^*$) single-electron excitation (in traditional $D_{4h}$ point group notation) and agrees well with the previous assignment discussed by Stillman and co-workers (*Inorg. Chem.* **1994**, *33*, 573−583). The TDDFT calculations also suggest a small energy gap for $b_{1u}/b_{2u}$ (Pc, $\pi^*$) orbital splitting and closeness of the $MLCT_1$ $e_g$ (Fe, $d_\pi$) → $b_{1u}$ (Pc, $\pi^*$) and $MLCT_2$ $e_g$ (Fe, $d_\pi$) → $b_{2u}$ (Pc, $\pi^*$) transitions. In the case of the $PcFeL_2$ complexes with phosphines as the axial ligands, additional degenerate charge-transfer transitions were observed between 450 and 500 nm. These transitions are dominated by $a_{2u}$ (Pc + L, $\pi$) → $e_g$ (Pc, $\pi^*$) single-electron excitations and are unique for the $PcFe(PR_3)_2$ complexes. The energy of the phthalocyanine-based $a_{2u}$ orbital has large axial ligand dependency and is the reason for a large energy deviation for B1 $a_{2u}$ (Pc + L, $\pi$) → $e_g$ (Pc, $\pi^*$) transition. The energies of the axial ligand-to-iron, axial ligand-to-phthalocyanine, iron-to-axial ligand, and phthalocyanine-to-axial ligand charge-transfer transitions were discussed on the basis of TDDFT calculations. Such LMCT, MLCT, and ILCT transitions have not been discussed in detail earlier and complicate the overall spectral profiles of $PcFeL_2$, PcFeL′L″, and $[PcFeX_2]^{2-}$ complexes and make the band assignments significantly more difficult.


https://doi.org/10.1021/acs.inorgchem.2c00721
*Inorg. Chem.* 2022, 61, 8250−8266

## COMPUTATIONAL DETAILS

**Experimental Section.** *Materials.* All solvents were purchased from commercial sources and purified using standard procedures. All compounds were prepared as described previously.[45,61]

*UV−Vis and MCD Spectroscopy.* All UV−vis spectra were collected on a Jasco V-770 spectrophotometer and MCD spectra were measured with a Jasco J-1500 CD spectrometer using a Jasco MCD-581 electromagnet operated at 1.0 T or a permanent magnet operated at 1.6 T. The completed MCD spectra were measured at 20 °C in parallel and antiparallel orientations with respect to the magnetic field. The MCD spectra were recorded in terms of mDeg = $[\theta]$ on the $y$-axis and were converted to molar ellipticity via $\Delta\varepsilon = \theta/(32980Blc)$, where $B$ is the magnetic field, $l$ is the path length (cm), and $c$ is the concentration (M).[116]

*Computational Aspects.* All calculations were run using Gaussian 16.[117] BP86[118,119] with Wachter's full-electron basis set[120] (Wf) for iron and the 6-311G(d) basis set[121] for the other atoms was used for all geometry optimizations. Similar to our previous report,[45] two geometries of the $[PcFe(Tz^{-})_2]^{2-}$ were considered in the calculations (Figure 1). Vibrational frequencies were calculated to ensure all geometries were local minima. Time-dependent density functional theory (TDDFT) with TPSSh,[122,123] O3LYP,[124] and MPWLYP[125] was used to calculate the first 80 excited states of each molecule. In addition, BP86, B3LYP,[126] PBE0,[127] M05,[128] M06,[129] M11,[130] MN12SX,[131] SOGGA11X,[132] wB97X,[133] TPSS/KCIS,[134] MPWKCIS,[135] X3LYP,[136] M11L,[137] wB97XD,[138] tHCTHThyb,[139] MN15,[140] HISSPBE,[141] CAM-B3LYP,[142] HSE0,[143] and LC-wHPBE[144] functionals were tested on a small group of compounds. The same basis sets as for the geometry optimizations were used for the TDDFT calculations. Single-point calculations using the same parameters as the TDDFT calculations were also performed. All calculations were run in solution using the PCM model,[145] with dichloromethane (DCM) or dimethylformamide (DMF) as the solvents. DCM was used with TPSSh, O3LYP, and MPWLYP, while DMF was only tested with MPWLYP. The compounds with butyl alkyl groups were shortened to methyl groups to minimize computational cost; so, $PcFe(PBu_3)_2$ was not calculated and PcFe $[P(OMe_3)]_2$ was calculated instead of $PcFe[P(OBu_3)]_2$. QMForge[146] was used for the molecular orbital composition analyses.

## ASSOCIATED CONTENT

### Supporting Information

The Supporting Information is available free of charge at https://pubs.acs.org/doi/10.1021/acs.inorgchem.2c00721.

Additional correlations, experimental, and computational data (PDF)

## AUTHOR INFORMATION


### Corresponding Author

**Victor N. Nemykin** − *Department of Chemistry, University of Manitoba, Winnipeg, Manitoba R3T 2N2, Canada; Department of Chemistry, University of Tennessee, Knoxville, Tennessee 37996, United States;* orcid.org/0000-0003-4345-0848; Email: vnemykin@utk.edu

### Authors

**Dustin E. Nevonen** − *Department of Chemistry, University of Manitoba, Winnipeg, Manitoba R3T 2N2, Canada*

**Laura S. Ferch** − *Department of Chemistry, University of Manitoba, Winnipeg, Manitoba R3T 2N2, Canada*

**Briana R. Schrage** − *Department of Chemistry, University of Tennessee, Knoxville, Tennessee 37996, United States*

Complete contact information is available at: https://pubs.acs.org/10.1021/acs.inorgchem.2c00721


### Notes

The authors declare no competing financial interest.

## ACKNOWLEDGMENTS

Generous support from the Minnesota Supercomputing Institute, CFI, NSF, WestGrid Canada, and the University of Tennessee to V.N.N. is greatly appreciated.

## REFERENCES


(1) Nemykin, V. N.; Tret'yakova, I. N.; Volkov, S. V.; Li, V. D.; Mekhryakova, N. G.; Kaliya, O. L.; Luk'yanets, E. A. Synthesis, structure and properties of coordination compounds of iron phthalocyanines and their analogues. *Russ. Chem. Rev.* **2000**, *69*, 325−346.

(2) Hanack, M. *Phthalocyanines: Properties and Applications*, Leznoff, C. C.; Lever, A. B. P., Eds.; VCH: New York, 1989; Vol. 2, pp 43−96.

(3) Ercolani, C.; Floris, B. *Phthalocyanines: Properties and Applications*, Leznoff, C. C.; Lever, A. B. P., Eds.; VCH: New York,1989; Vol. 2, pp 1−43.

(4) Taube, R. New aspects of the chemistry of transition metal phthalocyanines. *Pure Appl. Chem.* **1974**, *38*, 427−438.

(5) Sorokin, A. B. Phthalocyanine Metal Complexes in Catalysis. *Chem. Rev.* **2013**, *113*, 8152−8191.

(6) Kennedy, B. J.; Murray, K. S.; Zwack, P. R.; Homborg, H.; Kalz, W. Spin states in iron(III) phthalocyanines studied by Moessbauer, magnetic susceptibility, and ESR measurements. *Inorg. Chem.* **1986**, *25*, 2539−2545.

(7) Fitzgerald, J. P.; Lebenson, J. R.; Wang, G.; Yee, G. T.; Noll, B. C.; Sommer, R. D. Iron Tetraanthracenotetraazaporphyrins: Synthesis, Structural Characterization, Ligand Binding Properties, and Unexpected Selectivity of a Bis-"Bowl" Tetraazaporphyrin. *Inorg. Chem.* **2008**, *47*, 4520−4530.

(8) Fitzgerald, J. P.; Haggerty, B. S.; Rheingold, A. L.; May, L.; Brewer, G. A. Iron octaethyltetraazaporphyrins: synthesis, characterization, coordination chemistry, and comparisons to related iron porphyrins and phthalocyanines. *Inorg. Chem.* **1992**, *31*, 2006−2013.

(9) Oña-Burgos, P.; Casimiro, M.; Fernandez, I.; Navarro, A. V.; Fernandez-Sanchez, J. F.; Carretero, A. S.; Gutierrez, A. F. Octahedral iron(II) phthalocyanine complexes: multinuclear NMR and relevance as $NO_2$ chemical sensors. *Dalton Trans.* **2010**, *39*, 6231−6238.

(10) Valero-Navarro, A.; Fernandez-Sanchez, J. F.; Segura-Carretero, A.; Spichiger-Keller, U. E.; Fernandez-Gutierrez, A.; Ona, P.; Fernandez, I. Iron-phthalocyanine complexes immobilized in nanostructured metal oxide as optical sensors of NOx and CO-NMR and photophysical studies. *J. Porphyrins Phthalocyanines* **2009**, *13*, 616−623.

(11) Fernández-Sánchez, J.; Fernandez, I.; Steiger, R.; Beer, R.; Cannas, R.; Spichiger-Keller, U. E. Second-generation nanostructured metal oxide matrices to increase the thermal stability of CO and $NO_2$ sensing layers based on iron(II) phthalocyanine. *Adv. Funct. Mater.* **2007**, *17*, 1188−1198.

(12) Afanasiev, P.; Sorokin, A. B. $\mu$-Nitrido Diiron Macrocyclic Platform: Particular Structure for Particular Catalysis. *Acc. Chem. Res.* **2016**, *49*, 583−593.

(13) Wöhrle, D.; Baziakina, N.; Suvorova, O.; Makarov, S.; Kutureva, V.; Schupak, E.; Schnurpfeil, G. Phthalocyanine coatings

on silica and zinc oxide. Synthesis and their activities in the oxidation of sulfide. *J. Porphyrins Phthalocyanines* **2004**, *8*, 1390−1401.
(14) Wöhrle, D.; Suvorova, O.; Gerdes, R.; Bartels, O.; Lapok, L.; Baziakina, N.; Makarov, S.; Slodek, A. Efficient oxidations and photooxidations with molecular oxygen using metal phthalocyanines as catalysts and photocatalysts. *J. Porphyrins Phthalocyanines* **2004**, *08*, 1020−1041.
(15) Cailler, L. P.; Clemancey, M.; Barilone, J.; Maldivi, P.; Latour, J.-M.; Sorokin, A. B. Comparative Study of the Electronic Structures of $\mu$-Oxo, $\mu$-Nitrido, and $\mu$-Carbido Diiron Octapropylporphyrazine Complexes and Their Catalytic Activity in Cyclopropanation of Olefins. *Inorg. Chem.* **2020**, *59*, 1104−1116.
(16) Colomban, C.; Tobing, A. H.; Mukherjee, G.; Sastri, C. V.; Sorokin, A. B.; de Visser, S. P. Mechanism of Oxidative Activation of Fluorinated Aromatic Compounds by N-Bridged Diiron-Phthalocyanine: What Determines the Reactivity? *Chem. - Eur. J.* **2019**, *25*, 14320−14331.
(17) Neu, H. M.; Zhdankin, V. V.; Nemykin, V. N. Binuclear iron(III) phthalocyanine($\mu$-oxodimer)/tetrabutylammonium oxone: a powerful catalytic system for oxidation of hydrocarbons in organic solution. *Tetrahedron Lett.* **2010**, *51*, 6545−6548.
(18) Neu, H. M.; Yusubov, M. S.; Zhdankin, V. V.; Nemykin, V. N. Binuclear iron(III) phthalocyanine($\mu$-oxo-dimer)—catalyzed oxygenation of aromatic hydrocarbons with iodosylbenzene sulfate and iodosylbenzene as the oxidants. *Adv. Synth. Catal.* **2009**, *351*, 3168−3174.
(19) Geraskin, I. M.; Luedtke, M. W.; Neu, H. M.; Nemykin, V. N.; Zhdankin, V. V. Organic iodine(V) compounds as terminal oxidants in iron(III) phthalocyanine catalyzed oxidation of alcohols. *Tetrahedron Lett.* **2008**, *49*, 7410−7412.
(20) Griffin, J. R.; Wendell, C. I.; Garwin, J. A.; White, M. C. Catalytic C($sp^3$)-H Alkylation via an Iron Carbene Intermediate. *J. Am. Chem. Soc.* **2017**, *139*, 13624−13627.
(21) He, C.; Wu, Z.-Y.; Zhao, L.; Ming, M.; Zhang, Y.; Yi, Y.; Hu, J.-S. Identification of FeN4 as an Efficient Active Site for Electrochemical $N_2$ Reduction. *ACS Catal.* **2019**, *9*, 7311−7317.
(22) Hu, P.; Tan, M.; Cheng, L.; Zhao, H.; Feng, R.; Gu, W.-J.; Han, W. Bio-inspired iron-catalyzed oxidation of alkylarenes enables late-stage oxidation of complex methylarenes to arylaldehydes. *Nat. Commun.* **2019**, *10*, No. 2425.
(23) Govan, J.; Abarca, G.; Aliaga, C.; Sanhueza, B.; Orellana, W.; Cardenas-Jiron, G.; Zagal, J. H.; Tasca, F. Influence of cyano substituents on the electron density and catalytic activity towards the oxygen reduction reaction for iron phthalocyanine. The case for Fe(II) 2, 3, 9, 10, 16, 17, 23, 24-octa(cyano) phthalocyanine. *Electrochem. Commun.* **2020**, *118*, No. 106784.
(24) Praats, R.; Kaarik, M.; Kikas, A.; Kisand, V.; Aruvali, J.; Paiste, P.; Merisalu, M.; Leis, J.; Sammelselg, V.; Zagal, J. H.; et al.*et al.* Electrocatalytic oxygen reduction reaction on iron phthalocyanine-modified carbide-derived carbon/carbon nanotube composite electrocatalysts. *Electrochim. Acta* **2020**, *334*, No. 135575.
(25) Recio, F. J.; Gutierrez, C. A.; Venegas, R.; Linares-Flores, C.; Caro, C. A.; Zagal, J. H. Optimization of the electrocatalytic activity of MN4-macrocyclics adsorbed on graphite electrodes for the electrochemical oxidation of L-cysteine by tuning the M (II)/(I) formal potential of the catalyst: an overview. *Electrochim. Acta* **2014**, *140*, 482−488.
(26) Kuznetsova, N. A.; Kaliya, O. L. Heterogenized metallophthalocyanines for photodynamic microorganism inactivation: an overview of our experience. *Makrogeterotsikly* **2015**, *8*, 8−19.
(27) Gerasimova, G. K.; Yakubovskaya, R. I.; Pankratov, A. A.; Treshchalina, E. M.; Nemtsova, E. R.; Andreeva, T. N.; Venediktova, Y. B.; Plyutinskaya, A. D.; Bezborodova, O. A.; Sidorova, T. A.; Baryshnikov, A. B.; Kaliya, O. L.; Voroztsov, G. N.; Luzhkov, Y. M. Binary catalytic therapy: A new approach to treatment of malignant tumors. Results of pre-clinical and clinical studies. *Russ. J. Gen. Chem.* **2015**, *85*, 289−302.
(28) Nxele, S. R.; Nyokong, T. Conjugation of Azide-functionalised CdSe/ZnS Quantum Dots with Tetrakis(5-hexyn-oxy) Fe(II) phthalocyanine via Click Chemistry for Electrocatalysis. *Electrochim. Acta* **2016**, *194*, 26−39.
(29) Nxele, S. R.; Mashazi, P.; Nyokong, T. Electrode Modification Using Alkynyl Substituted Fe(II) Phthalocyanine via Electrografting and Click Chemistry for Electrocatalysis. *Electroanalysis* **2015**, *27*, 2468−2478.
(30) Maringa, A.; Mashazi, P.; Nyokong, T. Characterization of electrodes modified by one pot or step by step electro-click reaction and axial ligation of iron tetracarboxyphthalocyanine. *Electrochim. Acta* **2014**, *145*, 237−244.
(31) Coates, M.; Nyokong, T. Characterization of glassy carbon electrodes modified with carbon nanotubes and iron phthalocyanine through grafting and click chemistry. *Electrochim. Acta* **2013**, *91*, 158−165.
(32) Anderson, D. R.; Solntsev, P. V.; Rhoda, H. M.; Nemykin, V. N. How big is big? Separation by conventional methods, X-ray and electronic structures of positional isomers of bis-tert-butylisocyano adduct of 2(3), 9(10), 16(17), 23(24)-tetrachloro-3(2), 10(9), 17(16),24(23)-tetra(2, 6-di-iso-propylphenoxy)-phthalocyaninato iron(II) complex. *J. Porphyrins Phthalocyanines* **2016**, *20*, 337−351.
(33) Nemykin, V. N.; Purchel, A. A.; Spaeth, A. D.; Barybin, M. V. Probing the Electronic Properties of a Trinuclear Molecular Wire Involving Isocyanoferrocene and Iron(II) Phthalocyanine Motifs. *Inorg. Chem.* **2013**, *52*, 11004−11012.
(34) Hanack, M.; Knecht, S.; Polley, R.; Subramanian, L. R. Axially 1, 4-diisocyanobenzene bridged substituted iron(II) phthalocyanines and 2, 3-naphthalocyanines. *Synth. Met.* **1996**, *80*, 183−189.
(35) Schmid, G.; Witke, E.; Schlick, U.; Knecht, S.; Hanack, M. Substituent effects in soluble phthalocyaninatoiron(II) complexes. *J. Mater. Chem.* **1995**, *5*, 855−859.
(36) Ryu, H.; Knecht, S.; Subramanian, L. R.; Hanack, M. Synthesis and properties of bridged phthalocyaninatoiron(II) complexes with bidentate aliphatic isocyanides. *Synth. Met.* **1995**, *72*, 289−296.
(37) Hanack, M.; Knecht, S.; Witke, E.; Haisch, P. Synthesis and properties of soluble metallophthalocyanines. *Synth. Met.* **1993**, *55*, 873−878.
(38) Hanack, M.; Lange, A.; Grosshans, R. Tetrazine-bridged phthalocyaninato-metal complexes as semiconducting material. *Synth. Met.* **1991**, *45*, 59−70.
(39) Watkins, J. J.; Balch, A. L. Complexes of ferrous phthalocyanine with aromatic nitroso compounds, isocyanides, and phosphites. *Inorg. Chem.* **1975**, *14*, 2720−2723.
(40) Calderazzo, F.; Frediani, S.; James, B. R.; Pampaloni, G.; Reimer, K. J.; Sams, J. R.; Serra, A. M.; Vitali, D. Synthesis and Moessbauer spectroscopic studies of carbonyl derivatives of (phthalocyaninato) iron(II). *Inorg. Chem.* **1982**, *21*, 2302−2306.
(41) Calderazzo, F.; Pampaloni, G.; Vitali, D.; Collamati, I.; Dessy, G.; Fares, V. Bis adducts of phthalocyaninatoiron(II) with Group 6A axial donor atoms. Crystal and molecular structure of sulfur-bonded bis(dimethyl sulfoxide) phthalocyaninatoiron(II)-dimethyl sulfoxide (1/2). *J. Chem. Soc., Dalton Trans.* **1980**, 1965−1969.
(42) Calderazzo, F.; Vitali, D.; Pampaloni, G.; Collamati, I. Reaction of pentacarbonyliron with phthalonitrile in dimethylformamide and isolation of carbonyl derivatives of iron(II) phthalocyanine stabilized by group 6 donor atoms. *J. Chem. Soc., Chem. Commun.* **1979**, 221−222.
(43) Ohya, T.; Morohoshi, H.; Sato, M. Preparation and characterization of low-spin iron(II) porphyrin complexes with bis(phosphine) or bis(phosphite) axial ligands. *Inorg. Chem.* **1984**, *23*, 1303−1305.
(44) Sweigart, D. A. Axial ligand substitution in iron(II) phthalocyanine adducts: replacement of tri-n-butyl phosphite by tri-n-butylphosphine. *J. Chem. Soc., Dalton Trans.* **1976**, 1476−1477.
(45) Nemykin, V. N.; Nevonen, D. E.; Osterloh, W. R.; Ferch, L. S.; Harrison, L. A.; Marx, B. S.; Kadish, K. M. Application of Lever's $E_L$ Parameter Scale toward Fe(II)/Fe(III) versus Pc(2-)/Pc(1-) Oxidation Process Crossover Point in Axially Coordinated Iron(II) Phthalocyanine Complexes. *Inorg. Chem.* **2021**, *60*, 16626−16644.


https://doi.org/10.1021/acs.inorgchem.2c00721
*Inorg. Chem.* 2022, 61, 8250−8266

(46) Zanguina, A.; Bayo-Bangoura, M.; Bayo, K.; Ouedraogo, G. V. IR and UV−visible spectra of iron(II) phthalocyanine complexes with phosphine or phosphite. *Bull. Chem. Soc. Ethiop.* **2002**, *16*, 73−79.
(47) Nemykin, V. N.; Nevonen, D. E.; Ferch, L. S.; Shepit, M.; Herbert, D. E.; van Lierop, J. Accurate Prediction of Mössbauer Hyperfine Parameters in Bis-Axially Coordinated Iron(II) Phthalocyanines Using Density Functional Theory Calculations: A Story of a Single Orbital Revealed by Natural Bond Orbital Analysis. *Inorg. Chem.* **2021**, *60*, 3690−3706.
(48) Calderazzo, F.; Pampaloni, G.; Vitali, D.; Pelizzi, G.; Collamati, I.; Frediani, S.; Serra, A. M. Carbonyl derivatives of phthalocyaninatoiron(II), especially those containing Group VI axial donor atoms. Crystal and molecular structure of carbonyl(N, N-dimethylformamide) phthalocyaninatoiron(II) and Moessbauer studies of some of the products. *J. Organomet. Chem.* **1980**, *191*, 217−242.
(49) Lever, A. B. P.; Wilshire, J. P. Electrochemistry of iron phthalocyanine complexes in nonaqueous solvents and the identification of five-coordinate iron(I) phthalocyanine derivatives. *Inorg. Chem.* **1978**, *17*, 1145−1151.
(50) Jones, J. G.; Twigg, M. V. Axial ligand dissociation of phthalocyaninatoiron(II) adducts. Further evidence for a dissociative mechanism of substitution. *J. Chem. Soc., Dalton Trans.* **1978**, 1709−1714.
(51) Dale, B. W.; Williams, R. J. P.; Edwards, P. R.; Johnson, C. E. Moessbauer spectra of compounds containing iron(II) in strong-field tetragonal environments. *Trans. Faraday Soc.* **1968**, *64*, 620−629.
(52) Dale, B. W.; Williams, R. J. P.; Edwards, P. R.; Johnson, C. E. Nature of electric field-gradient tensor in strong-field tetragonal and pseudo-tetragonal complexes of divalent iron. *Trans. Faraday Soc.* **1968**, *64*, 3011−3013.
(53) Dale, B. W. Effect of axial ligands on the electronic absorption spectrum of phthalocyanineiron(II). *Trans. Faraday Soc.* **1969**, *65*, 331−339.
(54) Hanack, M.; Hirsch, A. Synthesis of bridged mixed valence macrocyclic compounds. *Synth. Met.* **1989**, *29*, F9−F14.
(55) Nemykin, V. N.; Polshina, A. E.; Chernii, V. Y.; Polshin, E. V.; Kobayashi, N. Synthesis, properties and Mossbauer spectra of bisaxially co-ordinated iron(II) phthalocyanine low-spin complexes: the first semi-quantitative explanation of the influence of the character of axial ligands on the spectral parameters. *J. Chem. Soc., Dalton Trans.* **2000**, 1019−1025.
(56) Nemykin, V. N.; Kobayashi, N.; Chernii, V. Y.; Belsky, V. K. Mossbauer, crystallographic, and density functional theoretical investigation of the electronic structure of bis-ligated low-spin iron(II) phthalocyanines. *Eur. J. Inorg. Chem.* **2001**, 733−743.
(57) Fernández, I.; Pregosin, P. S.; Albinati, A.; Rizzato, S.; Spichiger-Keller, U. E.; Nezel, T.; Fernandez-Sanchez, J. F. Solution NMR and X-ray structural studies on phthalocyaninatoiron complexes. *Helv. Chim. Acta* **2006**, *89*, 1485−1496.
(58) Nevonen, D. E.; Ferch, L. S.; Chernii, V. Y.; Herbert, D. E.; van Lierop, J.; Nemykin, V. N. X-Ray structures, Mossbauer hyperfine parameters, and molecular orbital descriptions of the phthalocyaninato iron(II) azole complexes. *J. Porphyrins Phthalocyanines* **2020**, *24*, 894−903.
(59) Ettorre, R.; Marton, D.; Russo, U.; Zanonato, P. Complexes of phthalocyaninatoiron(II) with diazoles. *J. Porphyrins Phthalocyanines* **2001**, *05*, 545−547.
(60) Ouedraogo, G. V.; More, C.; Richard, Y.; Benlian, D. Charge-transfer and Moessbauer spectra of axially substituted iron phthalocyanines. *Inorg. Chem.* **1981**, *20*, 4387−4393.
(61) Ough, E. A.; Stillman, M. J. Analysis of the absorption and magnetic circular dichroism spectra of iron(II) phthalocyanine. *Inorg. Chem.* **1994**, *33*, 573−583.
(62) Stillman, M. J.; Thomson, A. J. Orbital reduction factors in the lowest excited state of the phthalocyanine ring and their measurement by magnetic circular dichroism spectroscopy. *J. Chem. Soc., Faraday Trans. 2* **1974**, *70*, 805−814.
(63) Hanack, M.; Deger, S.; Lange, A. Bisaxially coordinated macrocyclic transition metal complexes. *Coord. Chem. Rev.* **1988**, *83*, 115−136.
(64) Schneider, O.; Hanack, M. Axially polymerized (phthalocyaninato) iron(II) with pyrazine, 4, 4′-bipyridine, 1, 4-diisocyanobenzene, or 1, 4-diazabicyclo[2.2.2] octane as bridging ligands; synthesis, characterization, and electrical conductivities. *Chem. Ber.* **1983**, *116*, 2088−2108.
(65) Hanack, M.; Hirsch, A.; Lehmann, H. Soluble oligomeric bridged phthalocyaninatoiron(II) complexes. *Angew. Chem., Int. Ed.* **1990**, *29*, 1467−1468.
(66) Hanack, M.; Duerr, K.; Lange, A.; Barcina, J. O.; Pohmer, J.; Witke, E. Synthesis of low band gap polymers—a challenge for organic chemists. *Synth. Met.* **1995**, *71*, 2275−2278.
(67) Hanack, M. Intrinsic semiconducting materials on phthalocyanine basis. *Turk. J. Chem.* **1998**, *22*, 13−22.
(68) Hanack, M.; Fiedler, M.; Subramanian, L. R. Phthalocyaninatoiron complexes with tridentate ligands. *Synth. Met.* **1999**, *100*, 123−130.
(69) Bayo, K.; Ouedraogo, G. V.; Terzian, G.; Benlian, D. UV−visible and IR spectra of iron(II) phthalocyanine polymer complexes linked by bis-pyridinato ligands. *Polyhedron* **1990**, *9*, 1087−1090.
(70) Ercolani, C.; Monacelli, F.; Dzugan, S.; Goedken, V. L.; Pennesi, G.; Rossi, G. X-ray crystal structure of $\mu$-oxo-bis[(1-methylimidazole) phthalocyaninatoiron(III)] and comments on the molecular structure and chemistry of oxo-bridged iron phthalocyaninate dimers. *J. Chem. Soc., Dalton Trans.* **1991**, 1309−1315.
(71) Janczak, J.; Kubiak, R. Pyrazine control of the supramolecular chemistry of iron(II) and cobalt (II) phthalocyanines. *CrystEngComm* **2010**, *12*, 3599−3606.
(72) Janczak, J.; Kubiak, R. Synthesis, thermal stability and structural characterization of iron(II) phthalocyanine complex with 4-cyanopyridine. *Polyhedron* **2007**, *26*, 2997−3002.
(73) Lever, A. B. P. Electrochemical parametrization of metal complex redox potentials, using the ruthenium(III)/ruthenium(II) couple to generate a ligand electrochemical series. *Inorg. Chem.* **1990**, *29*, 1271−1285.
(74) Alexiou, C.; Lever, A. B. P. Tuning metalloporphyrin and metallophthalocyanine redox potentials using ligand electrochemical ($E_L$) and Hammett ($\sigma_p$) parametrization. *Coord. Chem. Rev.* **2001**, *216−217*, 45−54.
(75) Lever, A. B. P.; Dodsworth, E. S. *Inorganic Electronic Structure and Spectroscopy*, Solomon, E. I.; Lever, A. B. P., Eds.; John Wiley & Sons, Inc., 1999; Vol. *II*, pp 227−289.
(76) Lever, A. B. P. The phthalocyanines-molecules of enduring value; a two-dimensional analysis of redox potentials. *J. Porphyrins Phthalocyanines* **1999**, *3*, 488−499.
(77) Vlček, A. Relation between spectral and redox properties of coordination compounds. *Electrochim. Acta* **1968**, *13*, 1063−1078.
(78) Goswami, S.; Chakravarty, A. R.; Chakravorty, A. Chemistry of ruthenium. 5. Reaction of trans-dihalobis[2-(arylazo)pyridine]-ruthenium(II) with tertiary phosphines: chemical, spectroelectrochemical, and mechanistic characterization of geometrically isomerized substitution products. *Inorg. Chem.* **1982**, *21*, 2737−2742.
(79) Chakravarty, A. R.; Chakravorty, A. Chemistry of ruthenium. Part 6. Bis(2,2′-bipyridine)(isonitrosoketonato)ruthenium(II) perchlorate monohydrate. Synthesis, spectra, and electrochemistry. *J. Chem. Soc., Dalton Trans.* **1982**, *9*, 1765−1771.
(80) Matsubara, T.; Ford, P. C. Some applications of cyclic voltammetry to the reactions and properties of ruthenium ammine complexes. Reduction potentials and rate studies. *Inorg. Chem.* **1976**, *15*, 1107−1110.
(81) Day, P.; Sanders, N. Spectra of complexes of conjugated lignads. I. Charge-transfer in phenanthroline complexes: energy shift on substitution. *J. Chem. Soc. A* **1967**, *10*, 1530−1536.
(82) Toma, H. E. Ion association and charge-transfer excitation between N-heterocyclic cations and cyanoiron complexes. *Can. J. Chem.* **1979**, *57*, 2079−2084.


https://doi.org/10.1021/acs.inorgchem.2c00721
*Inorg. Chem.* 2022, 61, 8250−8266

(83) Pombeiro, A. J. L.; Richards, R. L. The chemical oxidation and electronic spectra of the trans-bis[bis(diphenylphosphino)ethane]bis-(substituted isonitrile) metal complexes trans-[M(CNR)2-(Ph2PCH2CH2PPh2)2] (M = molybdenum or tungsten). *J. Organomet. Chem.* **1979**, *179*, 459−477.
(84) Brisset, J. L.; Biquard, M. Pentacyano(pyridine)ferrates(II) and −(III) and related compounds. *Inorg. Chim. Acta* **1981**, *53*, L125−L128.
(85) Shriver, D. F.; Posner, J. Bridge addition compounds. III. The influence of boron containing Lewis acids on electronic spectra, vibrational spectra, and oxidation potentials of some iron-cyanide complexes. *J. Am. Chem. Soc.* **1966**, *88*, 1672−1677.
(86) Dart, J. W.; Lloyd, M. K.; Mason, R.; McCleverty, J. A.; Williams, J. Properties of isocyanide ligands in metal complexes. Characterization and voltametric properties of bis(tertiary phosphine)tris(isonitrile) cobalt(I) complexes. *J. Chem. Soc., Dalton Trans.* **1973**, *17*, 1747−1751.
(87) Rillema, D. P.; Mack, K. B. The low-lying excited state in ligand $\pi$-donor complexes of ruthenium(II): mononuclear and binuclear species. *Inorg. Chem.* **1982**, *21*, 3849−3854.
(88) Ford, P. C.; Rudd, D. P.; Gaunder, R.; Taube, H. Synthesis and properties of pentaamminepyridineruthenium(II) and related pentaammineruthenium complexes of aromatic nitrogen heterocycles. *J. Am. Chem. Soc.* **1968**, *90*, 1187−1194.
(89) Johnson, C. R.; Shepherd, R. E. Metal-to-ligand charge-transfer spectra of pentacyanoruthenate(II) complexes of aromatic nitrogen heterocycles. *Inorg. Chem.* **1983**, *22*, 2439−2444.
(90) Ghosh, P.; Chakravorty, A. Hydroxamates of bis(2,2′-bipyridine)ruthenium: synthesis, protic, redox, and electroprotic equilibria, spectra, and spectroelectrochemical correlations. *Inorg. Chem.* **1984**, *23*, 2242−2248.
(91) Goswami, S.; Mukherjee, R.; Chakravorty, A. Chemistry of ruthenium. 12. Reactions of bidentate ligands with diaquabis[2-(arylazo)pyridine]ruthenium(II) cation. Stereoretentive synthesis and tris chelates and their characterization: metal oxidation, ligand reduction, and spectroelectrochemical correlation. *Inorg. Chem.* **1983**, *22*, 2825−2832.
(92) Sullivan, B. P.; Caspar, J. V.; Meyer, T. J.; Johnson, S. Hydrido carbonyl complexes of osmium(II) and ruthenium(II) containing polypyridyl ligands. *Organometallics* **1984**, *3*, 1241−1251.
(93) Saji, T.; Aoyagui, S. Polarographic studies on bipyridine complexes. II. Correlation between charge-transfer frequencies and oxidation potentials of tris(2,2′-bipyridine) complexes of iron, ruthenium, osmium, cobalt, and chromium. *J. Electroanal. Chem. Interfacial Electrochem.* **1975**, *60*, 1−10.
(94) Curtis, J. C.; Sullivan, B. P.; Meyer, T. J. Hydrogen-bonding-induced solvatochromism in the charge-transfer transitions of ruthenium(II) and ruthenium(III) ammine complexes. *Inorg. Chem.* **1983**, *22*, 224−236.
(95) Ohsawa, Y.; Hanck, K. W.; DeArmond, M. K. A systematic electrochemical and spectroscopic study of mixed-ligand ruthenium-(II) 2,2′-bipyridine complexes [Ru(bpy)3-nLn]2+ (n = 0, 1, 2, and 3). *J. Electroanal. Chem. Interfacial Electrochem.* **1984**, *175*, 229−240.
(96) Toma, H. E. Intervalence transfer in outer-sphere hexaammineruthenium(III)pentacyanoferrate(II) complexes. *J. Chem. Soc., Dalton Trans.* **1980**, *3*, 471−475.
(97) Curtis, J. C.; Meyer, T. J. Outer-sphere intervalence transfer. *J. Am. Chem. Soc.* **1978**, *100*, 6284−6286.
(98) Hennig, H.; Rehorek, A.; Ackerman, M.; Rehorek, D.; Thomas, P. Photocatalytic systems. XLIV. Intervalence charge transfer behavior of ion pair associates of octacyanomolybdate. *Z. Anorg. Allg. Chem.* **1983**, *496*, 186−196.
(99) Dodsworth, E. S.; Lever, A. B. P. Correlation of electronic charge transfer transitions and electrochemical potentials. The bipyrazine(tetracarbonyl) molybdenum(O) system in various solvents. *Chem. Phys. Lett.* **1984**, *112*, 567−570.
(100) Dodsworth, E. S.; Lever, A. B. P. Relationships between electronic spectroscopy and electrochemistry. A probe of reorganization energies. *Chem. Phys. Lett.* **1985**, *119*, 61−66.
(101) Lever, A. B. P.; Pickens, S. R.; Minor, P. C.; Licoccia, S.; Ramaswamy, B. S.; Magnell, K. Charge-transfer spectra of metallophthalocyanines: correlation with electrode potentials. *J. Am. Chem. Soc.* **1981**, *103*, 6800−6806.
(102) Vlcek, A. A.; Dodsworth, E. S.; Pietro, W. J.; Lever, A. B. P. Excited State Redox Potentials of Ruthenium Diimine Complexes; Correlations with Ground State Redox Potentials and Ligand Parameters. *Inorg. Chem.* **1995**, *34*, 1906−1913.
(103) Allard, M. M.; Odongo, O. S.; Lee, M. M.; Chen, Y.-J.; Endicott, J. F.; Schlegel, H. B. Effects of Electronic Mixing in Ruthenium(II) Complexes with Two Equivalent Acceptor Ligands. Spectroscopic, Electrochemical, and Computational Studies. *Inorg. Chem.* **2010**, *49*, 6840−6852.
(104) Dodsworth, E. S.; Lever, A. B. P. Correlations between electrochemical potentials and optical charge transfer energies in ruthenium bipyridine derivatives. *Chem. Phys. Lett.* **1986**, *124*, 152−158.
(105) Nemykin, V. N.; Lukyanets, E. A. The Key Role of the Peripheral Substituents in the Chemistry of Phthalocyanines. In *Handbook of Porphyrin Science*, Kadish, K. M.; Smith, K. M.; Guilard, R., Eds.; World Scientific: Singapore, 2010; Vol. *3*, pp 1−323.
(106) Nemykin, V. N.; Hadt, R. G. Influence of Hartree-Fock Exchange on the Calculated Moessbauer Isomer Shifts and Quadrupole Splittings in Ferrocene Derivatives Using Density Functional Theory. *Inorg. Chem.* **2006**, *45*, 8297−8307.
(107) Nemykin, V. N.; Basu, P. Comparative theoretical investigation of the vertical excitation energies and the electronic structure of $[Mo^{V}OCl_4]^-$: influence of basis set and geometry. *Inorg. Chem.* **2003**, *42*, 4046−4056.
(108) Belosludov, R. V.; Nevonen, D.; Rhoda, H. M.; Sabin, J. R.; Nemykin, V. N. Simultaneous Prediction of the Energies of Qx and Qy Bands and Intramolecular Charge-Transfer Transitions in Benzoannulated and Non-Peripherally Substituted Metal-Free Phthalocyanines and Their Analogues: No Standard TDDFT Silver Bullet Yet. *J. Phys. Chem. A* **2019**, *123*, 132−152.
(109) Martynov, A. G.; Mack, J.; May, A. K.; Nyokong, T.; Gorbunova, Y. G.; Tsivadze, A. Y. Methodological Survey of Simplified TD-DFT Methods for Fast and Accurate Interpretation of UV-Vis-NIR Spectra of Phthalocyanines. *ACS Omega* **2019**, *4*, 7265−7284.
(110) Zerner, M.; Gouterman, M. Porphyrins. IV. Extended Hueckel Calculations on Transition Metal Complexes. *Theor. Chim. Acta* **1966**, *4*, 44−63.
(111) Zerner, M.; Gouterman, M.; Porphyrins, V. Extended Hueckel Calculations on Vanadyl (VO2+) and Vanadium(II) Complexes. *Inorg. Chem.* **1966**, *5*, 1699−1706.
(112) Zerner, M.; Gouterman, M.; Porphyrins, X. Extended Hueckel Calculations on Alkaline Earth Complexes. *Theor. Chim. Acta* **1967**, *8*, 26−34.
(113) Sumimoto, M.; Kawashima, Y.; Hori, K.; Fujimoto, H. Theoretical investigation of the molecular and electronic structures and excitation spectra of iron phthalocyanine and its derivatives, FePc and FePcLn (L = Py, CN-; n = 1, 2). *Dalton Trans.* **2009**, 5737−5746.
(114) Ough, E.; Gasyna, Z.; Stillman, M. J. Photochemical, electrochemical, and chemical formation of the $\pi$-cation-radical species of magnesium phthalocyanine. Analysis of the absorption and MCD spectra of [MgPc(-1)].+. *Inorg. Chem.* **1991**, *30*, 2301−2310.
(115) Fukuda, T.; Homma, S.; Kobayashi, N. A highly deformed iron(II) low-spin phthalocyanine which shows two MLCT transitions beyond the Q-band. *Chem. Commun.* **2003**, 1574−1575.
(116) Galinato, M. G. I.; Spolitak, T.; Ballou, D. P.; Lehnert, N. Elucidating the Role of the Proximal Cysteine Hydrogen-Bonding Network in Ferric Cytochrome P450cam and Corresponding Mutants Using Magnetic Circular Dichroism Spectroscopy. *Biochemistry* **2011**, *50*, 1053−1069.
(117) Frisch, M. J.; Trucks, G. W.; Schlegel, H. B.; Scuseria, G. E.; Robb, M. A.; Cheeseman, J. R.; Scalmani, G.; Barone, V.; Petersson, G. A.; Nakatsuji, H.; Li, X.; Caricato, M.; Marenich, A. V.; Bloino, J.;


https://doi.org/10.1021/acs.inorgchem.2c00721
*Inorg. Chem.* 2022, 61, 8250−8266

Janesko, B. G.; Gomperts, R.; Mennucci, B.; Hratchian, H. P.; Ortiz, J. V.; Izmaylov, A. F.; Sonnenberg, J. L.; Williams-Young, D.; Ding, F.; Lipparini, F.; Egidi, F.; Goings, J.; Peng, B.; Petrone, A.; Henderson, T.; Ranasinghe, D.; Zakrzewski, V. G.; Gao, J.; Rega, N.; Zheng, G.; Liang, W.; Hada, M.; Ehara, M.; Toyota, K.; Fukuda, R.; Hasegawa, J.; Ishida, M.; Nakajima, T.; Honda, Y.; Kitao, O.; Nakai, H.; Vreven, T.; Throssell, K.; Montgomery, J. A., Jr.; Peralta, J. E.; Ogliaro, F.; Bearpark, M. J.; Heyd, J. J.; Brothers, E. N.; Kudin, K. N.; Staroverov, V. N.; Keith, T. A.; Kobayashi, R.; Normand, J.; Raghavachari, K.; Rendell, A. P.; Burant, J. C.; Iyengar, S. S.; Tomasi, J.; Cossi, M.; Millam, J. M.; Klene, M.; Adamo, C.; Cammi, R.; Ochterski, J. W.; Martin, R. L.; Morokuma, K.; Farkas, O.; Foresman, J. B.; Fox, D. J.; et al. *Gaussian 16*, revision B.01; Gaussian, Inc.: Wallingford, CT, 2016.

(118) Becke, A. D. Density-functional exchange-energy approximation with correct asymptotic behaviour. *Phys. Rev. A* **1988**, *38*, 3098−3100.

(119) Perdew, J. P. Density-functional approximation for the correlation energy of the inhomogeneous electron gas. *Phys. Rev. B* **1986**, *33*, 8822−8824.

(120) Wachters, A. J. H. Gaussian Basis Set for Molecular Wavefunctions Containing Third-Row Atoms. *J. Chem. Phys.* **1970**, *52*, 1033−1036.

(121) McLean, A. D.; Chandler, G. S. Contracted Gaussian basis sets for molecular calculations. 1. Second row atoms, Z = 11−18. *J. Chem. Phys.* **1980**, *72*, 5639−5648.

(122) Staroverov, V. N.; Scuseria, G. N.; Tao, J.; Perdew, J. P. Comparative assessment of a new nonempirical density functional: Molecules and hydrogen-bonded complexes. *J. Chem. Phys.* **2003**, *119*, 12129−12137.

(123) Tao, J. M.; Perdew, J. P.; Staroverov, V. N.; Scuseria, G. E. Climbing the density functional ladder: Nonempirical meta-generalized gradient approximation designed for molecules and solids. *Phys. Rev. Lett.* **2003**, *91*, No. 146401.

(124) Cohen, A. J.; Handy, N. C. Dynamic correlation. *Mol. Phys.* **2001**, *99*, 607−615.

(125) Schultz, N. E.; Zhao, Y.; Truhlar, D. G. Density functionals for inorganometallic and organometallic chemistry. *J. Phys. Chem. A* **2005**, *109*, 11127−11143.

(126) Becke, A. D. Density-functional thermochemistry. III. The role of exact exchange. *J. Chem. Phys.* **1993**, *98*, 5648−5652.

(127) Ernzerhof, M.; Perdew, J. P. Generalized gradient approximation to the angle-and system-averaged exchange hole. *J. Chem. Phys.* **1998**, *109*, 3313−3320.

(128) Zhao, Y.; Schultz, N. E.; Truhlar, D. G. Exchange-correlation functionals with broad accuracy for metallic and nonmetallic compounds, kinetics, and noncovalent interactions. *J. Chem. Phys.* **2005**, *123*, No. 161103.

(129) Zhao, Y.; Truhlar, D. G. The M06 suite of density functionals for main group thermochemistry, thermochemical kinetics, noncovalent interactions, excited states, and transition elements: two new functionals and systematic testing of four M06 functionals and twelve other functionals. *Theor. Chem. Acc.* **2008**, *120*, 215−241.

(130) Peverati, R.; Truhlar, D. G. Improving the accuracy of hybrid meta-GGA density functionals by range separation. *J. Phys. Chem. Lett.* **2011**, *2*, 2810−2817.

(131) Peverati, R.; Truhlar, D. G. Screened-exchange density functionals with broad accuracy for chemistry and solid-state physics. *Phys. Chem. Chem. Phys.* **2012**, *14*, 16187−16191.

(132) Peverati, R.; Zhao, Y.; Truhlar, D. G. Generalized Gradient Approximation that Recovers the Second-Order Density-Gradient Expansion with Optimized Across-the-board Performance. *J. Phys. Chem. Lett.* **2011**, *2*, 1991−1997.

(133) Chai, J. D.; Head-Gordon, M. Systematic optimization of long-range corrected hybrid density functionals. *J. Chem. Phys.* **2008**, *128*, No. 084106.

(134) Zhao, Y.; Lynch, B. J.; Truhlar, D. G. Multi-coefficient extrapolated density functional theory for thermochemistry and thermochemical kinetics. *Phys. Chem. Chem. Phys.* **2005**, *7*, 43−52.

(135) Zhao, Y.; González-García, N.; Truhlar, D. G. Benchmark database of barrier heights for heavy atom transfer, nucleophilic substitution, association, and unimolecular reactions and their use to test density functional theory. *J. Phys. Chem. A* **2005**, *109*, 2012−2018.

(136) Xu, X.; Goddard, W. A., III. The X3LYP extended density functional for accurate descriptions of nonbond interactions, spin states, and thermochemical properties. *Proc. Natl. Acad. Sci. U.S.A.* **2004**, *101*, 2673−77.

(137) Peverati, R.; Truhlar, D. G. M11-L: A local density functional that provides improved accuracy for electronic structure calculations in chemistry and physics. *J. Phys. Chem. Lett.* **2012**, *3*, 117−124.

(138) Chai, J. D.; Head-Gordon, M. Long-range corrected hybrid density functionals with damped atom-atom dispersion corrections. *Phys. Chem. Chem. Phys.* **2008**, *10*, 6615−6620.

(139) Boese, A. D.; Martin, J. M. L. Development of density functionals for thermochemical kinetics. *J. Chem. Phys.* **2004**, *121*, 3405−3416.

(140) Yu, H. S.; He, X.; Li, S.; Truhlar, D. G. MN15: A Kohn-Sham global-hybrid exchange-correlation density functional with broad accuracy for multi-reference and single-reference systems and noncovalent interactions. *Chem. Sci.* **2016**, *7*, 5032−5051.

(141) Heyd, J.; Scuseria, G. Efficient hybrid density functional calculations in solids: The HS-Ernzerhof screened Coulomb hybrid functional. *J. Chem. Phys.* **2004**, *121*, 1187−1192.

(142) Yanai, T.; Tew, D.; Handy, N. A new hybrid exchange-correlation functional using the Coulomb-attenuating method (CAM-B3LYP). *Chem. Phys. Lett.* **2004**, *393*, 51−57.

(143) Heyd, J.; Scuseria, G. E.; Ernzerhof, M. Hybrid functionals based on a screened Coulomb potential. *J. Chem. Phys.* **2003**, *118*, 8207−8215.

(144) Vydrov, O. A.; Scuseria, G. E. Assessment of a long range corrected hybrid functional. *J. Chem. Phys.* **2006**, *125*, No. 234109.

(145) Tomasi, J.; Mennucci, B.; Cammi, R. Quantum mechanical continuum solvation models. *Chem. Rev.* **2005**, *105*, 2999−3093.

(146) Tenderholt, A. L. *QMForge*, version 2.1; Standord University: Stanford, CA, 2011. https://qmforge.net/.



https://doi.org/10.1021/acs.inorgchem.2c00721
*Inorg. Chem.* 2022, 61, 8250−8266